NASA/TP—2001–210793

Magnetic Flux Compression Reactor Concepts for Spacecraft Propulsion and Power

(MSFC Center Director's Discretionary Fund Final Report; Part I, Project No. 99–24)

R.J. Litchford and G.A. Robertson
Marshall Space Flight Center, Marshall Space Flight Center, Alabama

C.W. Hawk, M.W. Turner, and S. Koelfgen
University of Alabama in Huntsville, Huntsville, Alabama

January 2001

The NASA STI Program Office...in Profile

Since its founding, NASA has been dedicated to the advancement of aeronautics and space science. The NASA Scientific and Technical Information (STI) Program Office plays a key part in helping NASA maintain this important role.

The NASA STI Program Office is operated by Langley Research Center, the lead center for NASA's scientific and technical information. The NASA STI Program Office provides access to the NASA STI Database, the largest collection of aeronautical and space science STI in the world. The Program Office is also NASA's institutional mechanism for disseminating the results of its research and development activities. These results are published by NASA in the NASA STI Report Series, which includes the following report types:

- TECHNICAL PUBLICATION. Reports of completed research or a major significant phase of research that present the results of NASA programs and include extensive data or theoretical analysis. Includes compilations of significant scientific and technical data and information deemed to be of continuing reference value. NASA's counterpart of peer-reviewed formal professional papers but has less stringent limitations on manuscript length and extent of graphic presentations.

- TECHNICAL MEMORANDUM. Scientific and technical findings that are preliminary or of specialized interest, e.g., quick release reports, working papers, and bibliographies that contain minimal annotation. Does not contain extensive analysis.

- CONTRACTOR REPORT. Scientific and technical findings by NASA-sponsored contractors and grantees.

- CONFERENCE PUBLICATION. Collected papers from scientific and technical conferences, symposia, seminars, or other meetings sponsored or cosponsored by NASA.

- SPECIAL PUBLICATION. Scientific, technical, or historical information from NASA programs, projects, and mission, often concerned with subjects having substantial public interest.

- TECHNICAL TRANSLATION. English-language translations of foreign scientific and technical material pertinent to NASA's mission.

Specialized services that complement the STI Program Office's diverse offerings include creating custom thesauri, building customized databases, organizing and publishing research results...even providing videos.

For more information about the NASA STI Program Office, see the following:

- Access the NASA STI Program Home Page at ***http://www.sti.nasa.gov***

- E-mail your question via the Internet to help@sti.nasa.gov

- Fax your question to the NASA Access Help Desk at (301) 621–0134

- Telephone the NASA Access Help Desk at (301) 621–0390

- Write to:
  NASA Access Help Desk
  NASA Center for AeroSpace Information
  7121 Standard Drive
  Hanover, MD 21076–1320
  (301)621–0390

NASA/TP—2001–210793

Magnetic Flux Compression Reactor Concepts for Spacecraft Propulsion and Power

(MSFC Center Director's Discretionary Fund Final Report; Part I, Project No. 99–24)

R.J. Litchford and G.A. Robertson
Marshall Space Flight Center, Marshall Space Flight Center, Alabama

C.W. Hawk, M.W. Turner, and S. Koelfgen
University of Alabama in Huntsville, Huntsville, Alabama

National Aeronautics and
Space Administration

Marshall Space Flight Center • MSFC, Alabama 35812

January 2001

Acknowledgments

The authors acknowledge the support of George C. Marshall Space Flight Center (MSFC),
National Aeronautics and Space Administration (NASA), and the NASA Institute for Advanced Concepts (NIAC).
This Technical Publication represents the Final Report (Part I) for MSFC Center Director's Discretionary Fund (CDDF)
Project No. 99–24. The NASA Principal Investigator was Ron J. Litchford, TD15/ASTP.

This technical publication has been reviewed and is approved.

Garry M. Lyles
Manager
TD15/ASTP
Marshall Space Flight Center

Available from:

NASA Center for AeroSpace Information
7121 Standard Drive
Hanover, MD 21076–1320
(301) 621–0390

National Technical Information Service
5285 Port Royal Road
Springfield, VA 22161
(703) 487–4650

TABLE OF CONTENTS

LIST OF FIGURES

LIST OF FIGURES (Continued)

LIST OF TABLES

LIST OF ACRONYMS AND SYMBOLS

BSCCO	$Bi_2Sr_2CaCu_2O_x$
C4	composition–4
D	deuterium
HEDM	high-energy density matter
He	isotopes of helium
HTSC	high-temperature superconductor
MHD	magnetohydrodynamics
P	products
R	reactants
SMES	superconducting magnet energy storage
T	tritium

NOMENCLATURE

a	inner radius of tube
b	outer radius of tube
B_{app}	external applied magnetic field
$B_{c,1}$	first critical field level
$B_{c,2}$	second critical field level
B_{ind}	induced magnetic field
B_{surf}	surface flux density
c	speed of light
C_a	contour of armature surface
C_s	contour of stator surface
d	thickness of the stator
D_m	magnetic diffusivity
E	electric field
E_a	electric field in armature
E_s	electric field in stator
f	mathematical function
f_b	burn fraction
f_p	pulse rate
g	geometrical form factor
g_0	gravitational field of Earth

NOMENCLATURE (Continued)

H	magnetic intensity
H_0	initial magnetic intensity
H_{surf}	magnetic intensity at stator surface
i	instantaneous current
i_0	initial current
I_{sp}	specific impulse
j	current density
j_a	armature current density
j_s	stator current density
J_n	Bessel function of the first kind of order n
L	inductance
L_0	characteristic length of the reactor; initial inductance
L_g	time-varying generator inductance
L_L	fixed load inductance
m_i	mass of ion i
m_p	pellet mass
m_R	mass of reactants
N_i	number of ion species
P_L	power delivered to load
$r_a(t)$	time-dependent radius of the plasma armature
r_i	initial radius of the armature

NOMENCLATURE (Continued)

r_s	internal radius of the magnetic flux containment stator
r_t	turnaround radius
R	electrical resistance
R_m	magnetic Reynolds number
s_ϕ	flux skin depth
$s_{\phi,a}$	flux skin depth in armature
$s_{\phi,s}$	flux skin depth in stator
t	time
T	average thrust
u_0	characteristic plasma velocity
u_a	armature velocity
u_D	detonation velocity
$\overline{u}_i$	velocity of ion i
u_i	average ion velocity
V_0	flux containment volume at the beginning of armature expansion
V_L	load voltage
V_t	flux containment volume at the turnaround point
w_D	specific energy of detonation
W_0	initial energy stored in the load
W_a	energy dissipated in the armature
W_{elec}	extracted electrical energy

NOMENCLATURE (Continued)

W_{jet}	propulsive jet energy of the exhaust
W_k	kinetic energy
W_L	energy delivered to load
$W_{m,0}$	original magnetic field energy in the reaction chamber
$W_{m,t}$	magnetic field energy at the turnaround point
W_s	energy dissipated in the stator circuit
Y_n	Bessel function of the second kind of order n
z	height of the reaction chamber
α	fusion mass fraction
α_n	roots of equation (74)
Δm	total mass defect for the fusion reaction
Δt_p	characteristic time defining the penetration time of the magnetic field through the stator
ζ	distance parameter
η	energy conversion efficiency
η_j	magnet nozzle efficiency
η_k	global energy conversion efficiency
λ	flux coefficient
μ	magnetic permeability
ξ	armature expansion ratio
ρ_D	density of detonable material
σ	electrical conductivity

NOMENCLATURE (Continued)

σ_0	characteristic electrical conductivity
τ_1	characteristic time for field diffusion through hollow tube
τ_c	characteristic time for field compression
τ_D	characteristic time defining the penetration time of the magnetic field through the detonation plasma
ϕ	magnetic flux
ϕ_{diff}	diffused magnetic flux

TECHNICAL PUBLICATION

MAGNETIC FLUX COMPRESSION REACTOR CONCEPTS FOR SPACECRAFT PROPULSION AND POWER

1. INTRODUCTION

Driven by the desire for fast, efficient interplanetary transport, NASA has set a number of ambitious mission goals for future space flight. These goals include accomplishing missions to Mars within months rather than years and improving propulsion capability by a factor of 10 within 15 yr. These criteria can be roughly translated into a specific power goal of 10 kW/kg for the onboard powerplant and a specific impulse (I_{sp}) goal of 10,000 sec in combination with a thrust-to-mass ratio (acceleration) in excess of 10^{-3} g for the spacecraft propulsion system. The principal technical challenge is the development of propulsion systems exhibiting rapid acceleration and very high I_{sp} attributes.

Unfortunately, most highly efficient propulsion systems which are within the capabilities of present day technologies are either very heavy or yield very low impulse, such that the acceleration time to final velocity is too long to be of lasting interest. One exception, the nuclear thermal thruster, could achieve the desired acceleration but would require inordinately large propellant-to-payload mass ratios to reach the range of desired final velocities.

A particularly promising alternative approach, among several competing concepts that are beyond our modern technical capabilities, is a low-yield thermonuclear pulse thruster.[1–14] In this scheme, neutron-lean microfusion detonations form an expanding diamagnetic plasma cloud that compresses the magnetic flux within a semienclosed reactor structure. The plasma expansion is ultimately reversed by increasing magnetic pressure, and the detonation products are then collimated and expelled by a magnetic nozzle. The charged-particle expansion velocity in these detonations can be on the order of 10^6–10^7 m/sec and if effectively collimated by a magnetic nozzle, can yield the I_{sp} and acceleration levels needed for practical interplanetary flight.

Methods for inductively extracting electrical power from the compressed magnetic field can also be envisioned. This is an integral component of the scheme since the energy needed to power the standoff drivers for the subsequent detonation is extremely high. Furthermore, an indirect mode of operation is conceivable in which a detonation-driven electric power reactor is used to drive high-power electric thrusters.

Magnetic flux compression concepts merit reassessment for spacecraft applications, based on modern developments in target and reactor design principles. For example, these schemes could capitalize on recent advances in target technologies including inertial confinement fusion,[15] staged microfusion

schemes,[4,14,16,17] magnetized target fusion,[18,19] and fast ignition antimatter-initiated nuclear detonations.[20–22] It is also conceivable that chemical detonations utilizing advanced high-energy density matter (HEDM) charges could attain limited success if the resulting plasma clouds demonstrate the requisite diamagnetic properties.

Moreover, inductive storage power reactors based on field compression processes have been proposed as a prime pulse power source for high current standoff drivers and as a direct conversion topping cycle for pulsed fusion systems.[23–28] In comparison with capacitor banks, inductive energy storage devices are generally more compact and less costly and avoid the need for initial opening switches in the pulse-forming line. The possible utilization of high-temperature superconductors as a flux compression reactor surface appears to offer attractive advantages as well.

The objective of this work is to assess the system-level performance and engineering challenges of field compression reactors as applicable to interplanetary spacecraft. In particular, special attention is devoted to devices which compress the field between a detonation plasma armature and a superconducting stator.

2. FIELD COMPRESSION REACTOR CONCEPTS

Magnetic flux compression reactors are based on a multistep energy conversion process as follows: chemical/nuclear → kinetic → electrical → kinetic. The initial detonation charge is first transformed into the kinetic energy of a moving conductive armature. This kinetic energy is then transformed into electrical energy as the armature compresses an initial seed magnetic flux against a highly conductive stator surface. More specifically, a fraction of the energy is temporarily stored in a rapidly increasing magnetic field while a portion is extracted from the induced stator current as useful electrical power. If the kinetic energy of the armature is fully expended without destroying the device, then the compressed magnetic field can reverse the armature motion and return the stored electromagnetic energy as kinetic energy of the armature. The reaccelerated armature can then be expelled from the device for direct thrust production. Of course, all of these processes are subjected to conversion inefficiencies associated with nonideal losses.

In reactors of this type, magnetic flux is trapped between the fast-moving armature and the stationary stator because of circulating currents that are induced within the field compression surfaces. In fact, the magnetic flux can be trapped only if the armature and stator have electrical conductivities that are high enough to resist magnetic field penetration during the field compression process. This criterion naturally leads to consideration of highly conductive detonation sources (i.e., fusion plasma) and highly conductive stator materials (i.e., superconductors).

From the viewpoint of global energy conservation, these reactors obey the relation:

$$W_{jet} + W_{elec} = W_k - W_a - W_s = \eta_k W_k \quad , \tag{1}$$

where W_{jet} is the propulsive jet energy of the exhaust, W_{elec} is the useful extracted electrical energy, W_k is the initial kinetic energy of the detonation charge, W_a is the energy dissipated in the armature, W_s is the energy dissipated in the stator circuit, and η_k is a global energy conversion efficiency.

Ideally, the energy conversion efficiency can exceed 80 percent, but this value could be reduced substantially by real plasma processes such as flute instabilities, electron Joule heating effects, and field-aligned ion flow due to the ambipolar potential. Furthermore, the magnetic field configuration and reactor chamber design plays a significant role in terms of magnetic diffusion losses and magnetic flux compression efficiency.

For a pure electric power reactor, one is interested in achieving the highest possible W_{elec} with little concern for propulsive performance. For a propulsive reactor, one is interested in achieving the highest possible W_{jet} while also extracting the minimum necessary electrical energy that is needed to ignite the subsequent detonation. Two reactor design concepts suitable for spacecraft applications are discussed in section 2.1.

2.1 Propulsion Reactor

The typical propulsion reactor concept is based on a concave surface around which magnet coils are situated to form a magnetic mirror. In addition, because most pulse fusion schemes require a large amount of driver energy, these reactors almost always include a generator coil for electrical power generation. The Daedalus-class magnetic reaction chamber exemplifies this highly integrated approach.[6,7] In this technical paper, a slight variation on the Daedalus theme in which a bulk-processed, high-temperature superconductor acts as the reaction chamber wall is considered. This concept is illustrated in figure 1.

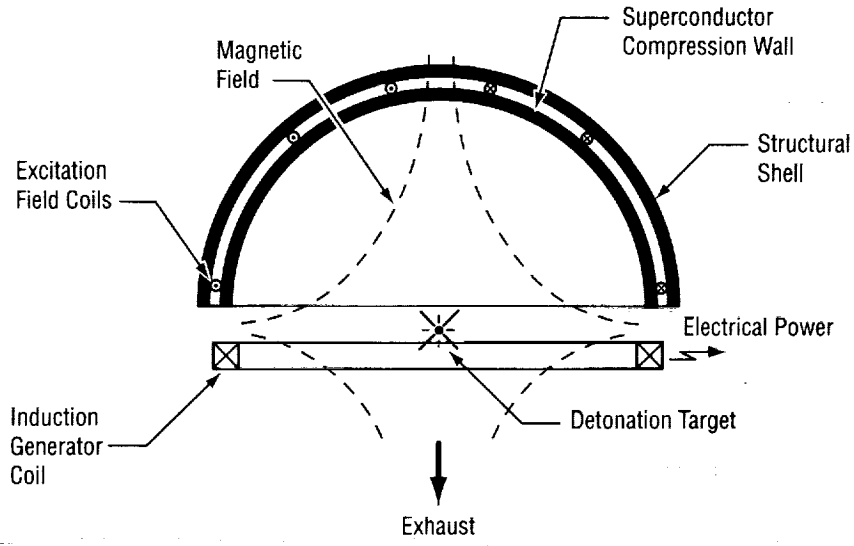

Figure 1. Magnetic flux compression reactor concept for integrated space propulsion and power.

In this concept, the plasma armature expands against a rearward-diverging magnetic field provided by a set of superconducting coils. The magnetic flux is trapped and compressed between the plasma and a high-temperature superconductor (HTSC) reaction chamber wall (i.e., stator). At some point, the expansion process is reversed and the increased magnetic pressure acting on the plasma forces it out the rear of the reaction chamber. The compressed magnetic field also produces a magnetic pressure on the reaction chamber wall, yielding a forward-thrust component. Electrical power is extracted from the flux compression process using an inductive pickup coil located at the exit of the reaction chamber.

By introducing an HTSC stator, it should be possible to reduce flux diffusion losses, reduce the minimum seed field, and reduce the overall size of the reaction chamber. The hoped-for result is a compact, low-weight integrated propulsion and power reactor driven by low-yield nuclear fusion detonation pulses that can yield acceptable interplanetary trip times while carrying sufficient payload to perform meaningful missions.

A nuclear pulse system based on this scheme can provide performance levels in the required regime of both high jet power and high I_{sp}. Along these lines, it is instructive to compute the theoretical performance limits that can be achieved for various fusion fuels.

2.1.1 Energetics

Starting with the assumption that after the nuclear reactions are quenched by the hydrodynamic disassembly, the fusion energy is averaged by collisions among all the particles in the plasma including the blowoff mass which did not undergo reaction. After complete thermalization, the energy per ion is the same throughout the fireball and the following relationship for energy conservation can be written:

$$\frac{1}{2} m_i u_i^2 = \frac{f_b \Delta m c^2}{N_i} \quad , \tag{2}$$

where m_i is the mass of ion i, u_i is the velocity of ion i, f_b is the burn fraction, Δm is the total mass defect for the fusion reaction, c is the speed of light, and N_i is the number of ion species generated per reaction. Neutrons are neglected because they carry no charge. Only the momentum of charge particles can be electromagnetically manipulated for direct thrust production. By introducing a parameter for the mass fraction that is converted to energy by the reaction ($\alpha = \Delta m / m_R$), it is possible to write eq. (2) in the form:

$$\frac{1}{2} m_i u_i^2 = \frac{f_b \alpha m_R c^2}{N_i} \quad , \tag{3}$$

where $m_R = \sum_R m_i$. From momentum conservation considerations, the following relationship is obtained:

$$\overline{m}_i \overline{u}_i = \frac{1}{2}\left[(1 - f_b)\sum\nolimits_R m_i u_i + f_b \sum\nolimits_P m_i u_i\right] \quad , \tag{4}$$

where the summations are over the reactants (R) and the products (P) and the overbar denotes an average over all ion species. Equation (3) can now be used to eliminate u_i on the right-hand side of eq. (4), such that an expression for the effective ion expansion velocity as a function of the burn fraction:

$$\overline{u}_i = \left[(1 - f_b)\sum\nolimits_R \sqrt{m_i} + f_b \sum\nolimits_P \sqrt{m_i}\right] \frac{1}{\sqrt{2}\overline{m}_i} \sqrt{\frac{f_b \alpha m_R c^2}{N_i}} \quad , \tag{5}$$

where the mean ion mass is defined by

$$\overline{m}_i = \frac{1}{2}\left[(1 - f_b)\sum\nolimits_R m_i + f_b \sum\nolimits_P m_i\right] \quad . \tag{6}$$

The theoretical I_{sp} may now be computed by noting that

$$I_{sp} = \frac{I}{\overline{m}_i} = \frac{\overline{m}_i \overline{u}_i}{\overline{m}_i} = \overline{u}_i \quad , \tag{7}$$

or when referenced to the Earth's gravitational field,

$$I_{sp} = \frac{\bar{u}_i}{g_0} \quad , \tag{8}$$

where $g_0 = 9.81$ m/s^2.

The nuclear fusion reactions of practical interest involve isotopes of hydrogen such as deuterium (D) and tritium (T) and isotopes of helium (He). These reactions are given in table 1 where the subscripts denote the nuclear charge (i.e., number of protons) and the superscripts denote the atomic mass number (i.e., total number of nucleons). The proton and neutron branches of the D-D reaction have similar valued cross sections such that each branch consumes roughly 50 percent of the fuel. The energy yield parameters for the various fusion reactions are given in table 2. It is important to note that the D-T and D-D reactions have larger fusion cross sections than the D-He reaction and are easier to ignite; however, they release approximately 80 percent and 35 percent, respectively, of the reaction energy in the form of neutrons which are useless for flux compression and wasteful for space propulsion applications, since they cannot be manipulated by electromagnetic means.

Table 1. Nuclear fusion reactions of major practical interest.

D-D	$_1D^2 + {}_1D^2$	$\rightarrow$	$_1T^3$(1.01 MeV) + $_1p^1$(3.02 MeV)	[W = 4.03 MeV]
		$\rightarrow$	$_2He^3$(0.82 MeV) + $_0n^1$(2.45 MeV)	[W = 3.27 MeV]
D-T	$_1D^2 + {}_1T^3$	$\rightarrow$	$_2He^4$(3.5 MeV) + $_0n^1$(14.1 MeV)	[W = 17.6 MeV]
D-He	$_1D^2 + {}_2He^3$	$\rightarrow$	$_2He^4$(3.6 MeV) + $_1p^1$(14.7 MeV)	[W = 18.3 MeV]

Table 2. Energy yield for major fusion fuels.

Fuel	Reaction Products	w (J/kg)	α
D-D	$_1T^3$, $_1p^1$	9.9×10^{13}	1.1×10^{-3}
D-D	$_2He^3$, $_0n^1$	8.1×10^{13}	9.0×10^{-4}
D-T	$_2He^4$, $_0n^1$	3.38×10^{14}	3.75×10^{-3}
D-He	$_2He^4$, $_1p^1$	3.52×10^{14}	3.91×10^{-3}

Practical considerations compel the use of D-He as a fusion fuel for space propulsion. Although the required ignition energy is substantially higher for D-He, the reaction products will consist predominately of charged particles, which can be electromagnetically manipulated. Of course, there will always be some neutron production due to D-D reactions of the primary fuel and D-T reactions between the primary D and secondary T. However, calculations indicate that the number of neutron reactions can be <5 percent of the D-He reactions.[6]

Using the parameters summarized in tables 1 and 2, it is possible to compute the effective detonation expansion velocity and theoretical I_{sp} for the D-He fusion reaction of interest using eqs. (5) and (8). The results of these calculations are shown in figure 2 as a function of the burn fraction. Detailed inertial confinement fusion calculations indicate that it should be possible to achieve a burn fraction of at least 10 percent, yielding an effective expansion velocity approaching 10^7 m/sec. The I_{sp} in this range will be on the order of 10^6 sec. Note that these calculations represent only a theoretical upper limit.

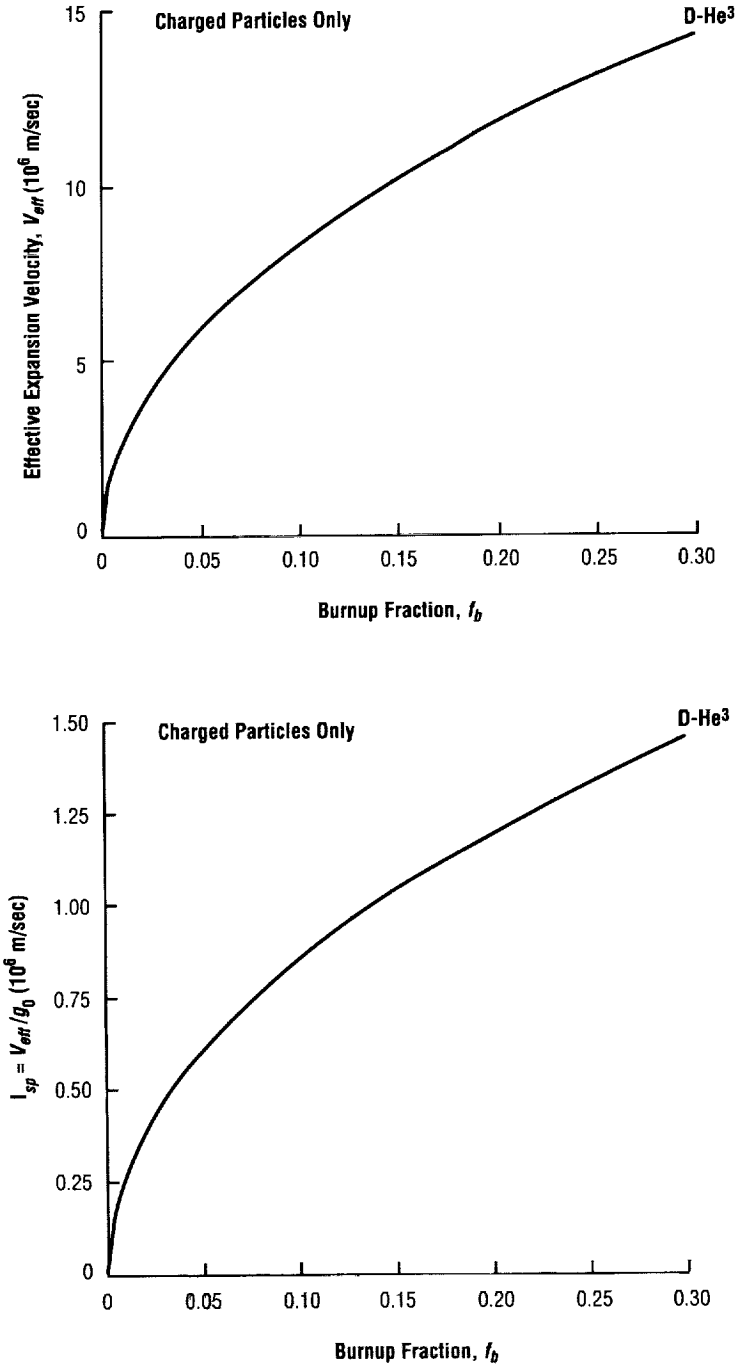

Figure 2. Computed effective expansion velocity and I_{sp} for a D-He fusion detonation.

2.1.2 Thrust Performance

The average thrust (T) produced by a nuclear pulse engine is governed by the pulse rate (f_p), the pellet mass (m_p), the magnetic nozzle efficiency (η_j), and the effective expansion velocity as defined by the following relationship:

$$T = \eta_j f_p m_p \bar{u}_i \quad . \tag{9}$$

The average thrust of a propulsive reactor has been calculated assuming a 200-MJ yield fusion detonation of D-He, a pulse rate of 100 Hz, and a nozzle efficiency of 65 percent. The results are shown as a function of burn fraction in figure 3. When assuming a constant energy yield, the average thrust decreases with increasing burn fraction, since the pellet mass is decreasing with increasing burn efficiency. By the same token, the I_{sp} will increase with increasing burn efficiency. At a practical burn fraction of 10 percent, the average thrust is ≈3 kN and the I_{sp} is approximately 8×10^5 sec for the assumed parameter values.

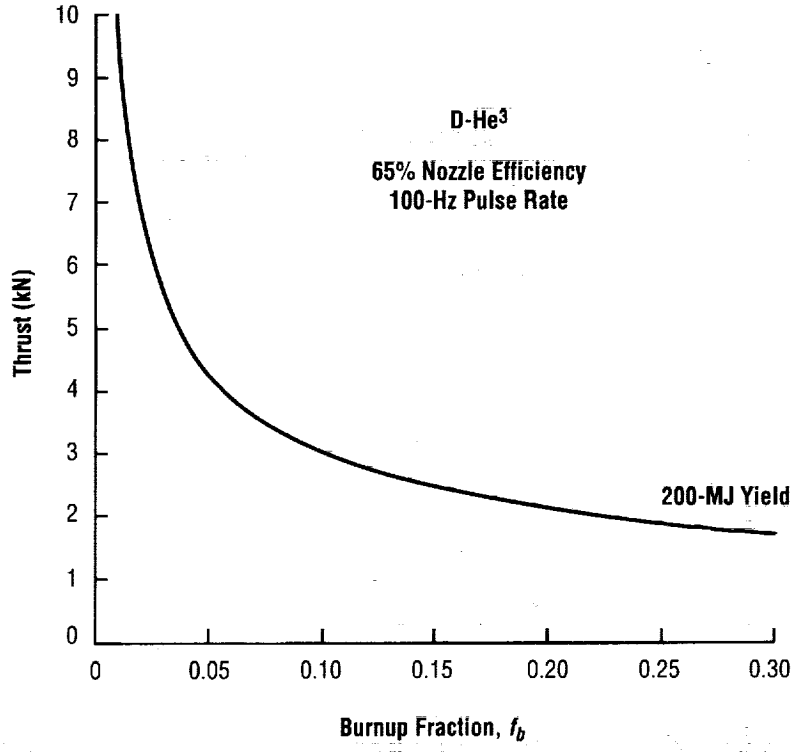

Figure 3. Average reactor thrust versus burnup fraction assuming 200-MJ fusion detonations of D-He at a pulse rate of 100 Hz with a nozzle efficiency of 65 percent.

2.2 Power Reactor

A schematic of a simple radial-mode power reactor with inductively coupled circuits for power extraction is shown in figure 4. Although other geometries are conceivable (e.g., spherical), the radial reactor is more amenable to power production with neutralized thrust. In the radial configuration, the generator consists of three nested shells. The innermost shell is the pickup (stator) coil in which electrical power is inductively extracted from the flux compression process. It is anticipated that the pickup coil will be fabricated from HTSC material. The pickup coil is surrounded by a conductive shielding shell which may or may not be fabricated from an HTSC material in bulk processed form. The purpose of the shielding shell is to minimize induced current transients in the outer magnet coil whose function is to produce the initial seed flux in the generator.

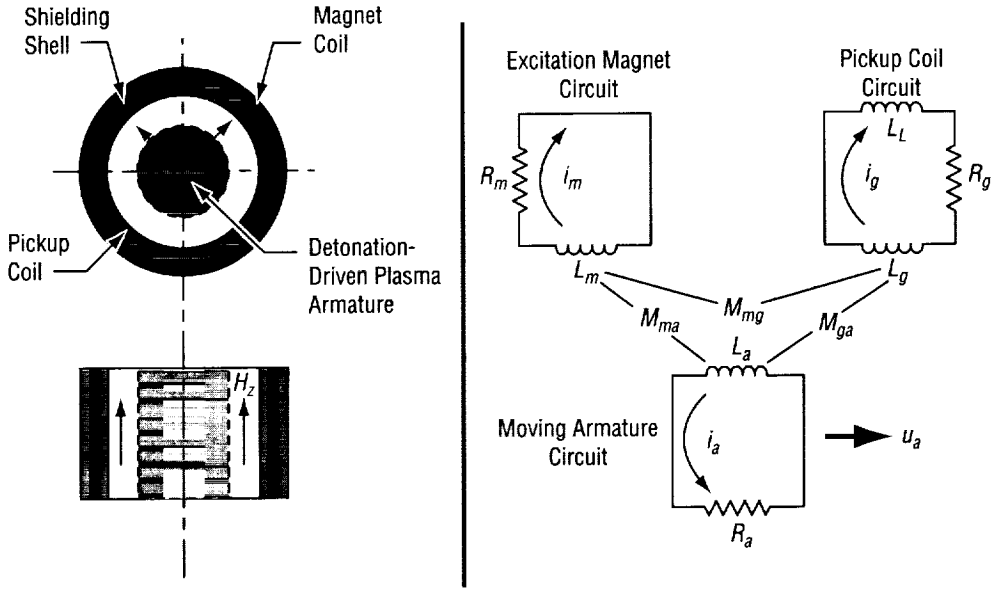

Figure 4. Schematic of radial-mode magnetic flux compression power reactor with inductively coupled power extraction circuit.

If a nuclear detonation is used as the plasma source, a target pellet would be fired into the reaction chamber and ignited by a high-energy driver (i.e., laser beam or particle beam). If a chemical detonation is used as the plasma source, the explosive component could either be fired into the reaction chamber as a target pellet or directly inserted as an expendable cartridge.

In practice, all of the individual circuit elements will interact inductively. The coupling of these circuits is defined by the mutual inductance between the various elements. In a good engineering design, the mutual inductance between the excitation magnetic coil and the other circuit elements in the system will be negligible. For good energy conversion efficiency, the goal is to cause an effective reduction in generator self-inductance through an increase in the mutual inductance between the expanding armature and the pickup coil. In this way, it is not necessary to deform the circuits.

As it is envisioned, the power reactor would embody superconducting magnet energy storage (SMES) technology as a means of inductively storing the extracted electrical power. This approach, illustrated in figure 5, is much more compact, lower in weight, and lower in cost than capacitive energy storage technologies. In this system, the load coil would be a normal metal conductor while the storage coil would be a superconductor. The SMES coil would be open during pulse generation and immediately closed at peak current. An operating reactor must be expected to supply its own operational power requirements, and this system would be able to supply the on-demand pulse power needed for ignition of the subsequent detonation. If the electrical energy is to be used in a normal power grid, several storage coils could be incorporated into the design such that continuous direct current power can be conditioned and bussed throughout the spacecraft.

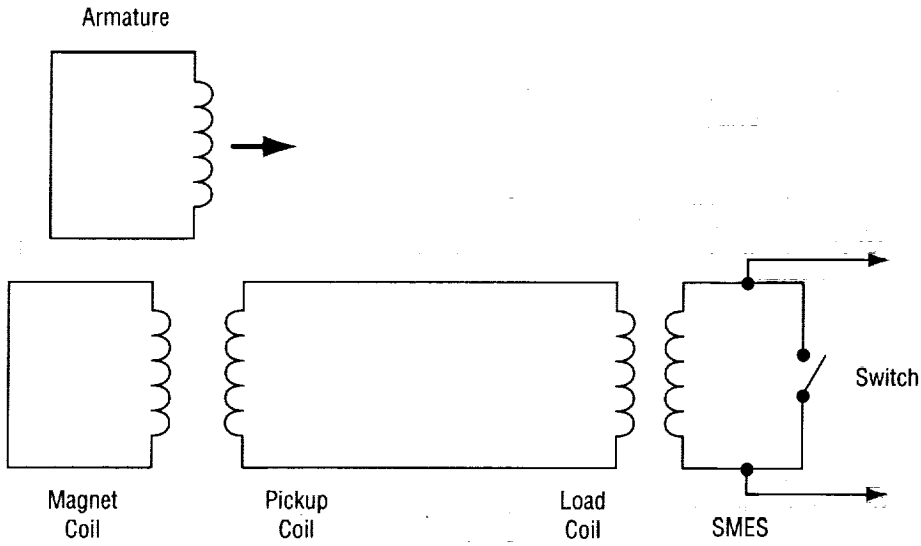

Figure 5. Schematic of SMES circuit coupled to a flux compression power reactor.

2.2.1 Simplified Circuit Analysis

The flux compression reactor circuit is illustrated schematically in figure 6. For simplicity, the generator is depicted as a single-turn induction coil connected to a single-turn load coil. The induction coil serves as a stator while the expanding plasma serves as an armature. The circuit diagram for the generator is shown as a time-varying generator inductance (L_g) connected to a fixed load inductance (L_L) with a resistive loss component (R).

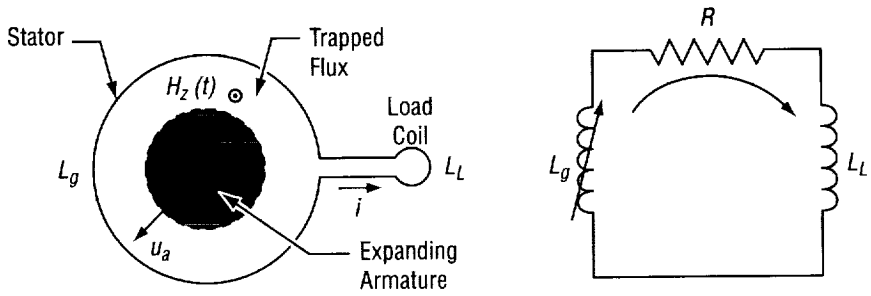

Figure 6. Schematic of flux compression reactor electrical circuit.

The principle of operation is as follows: (1) Seed flux injection, (2) ignition of centrally located charge, (3) detonation-driven expansion of the plasma armature, (4) magnetic flux trapping between the plasma armature and the stator coil with magnetic flux diffusion into both the stator and armature, (5) rapid field compression as the kinetic energy of the plasma is transformed into magnetic pressure, and (6) forced reduction in generator inductance yielding a fast rise time current pulse.

The circuit equation for the generator may be written in differential form as

$$\frac{d}{dt}(Li) + Ri = 0 \quad , \tag{10}$$

where $L = L_g + L_L$ and i is the instantaneous current. Solving for the current, the following is obtained:

$$i = \frac{L_0 i_0}{L} \exp\left\{-\int_0^t (R/L)dt\right\} \tag{11}$$

and find that the current varies inversely with the generator inductance. It is convenient to rewrite eq. (11) in terms of a flux coefficient λ:

$$\lambda = \frac{\phi}{\phi_0} = \frac{Li}{L_0 i_0} = \exp\left\{-\int_0^t (R/L)dt\right\} < 1 \quad , \tag{12}$$

where ϕ is the magnetic flux. Thus, λ is a measure of flux compression efficiency and quantifies the magnetic flux diffusion losses into the stator and the armature through a negative exponential function. These magnetic diffusion processes are illustrated in figure 7. It should be noted that the expression for the flux coefficient demonstrates that flux diffusion losses can be effectively expressed in terms of a resistive circuit component.

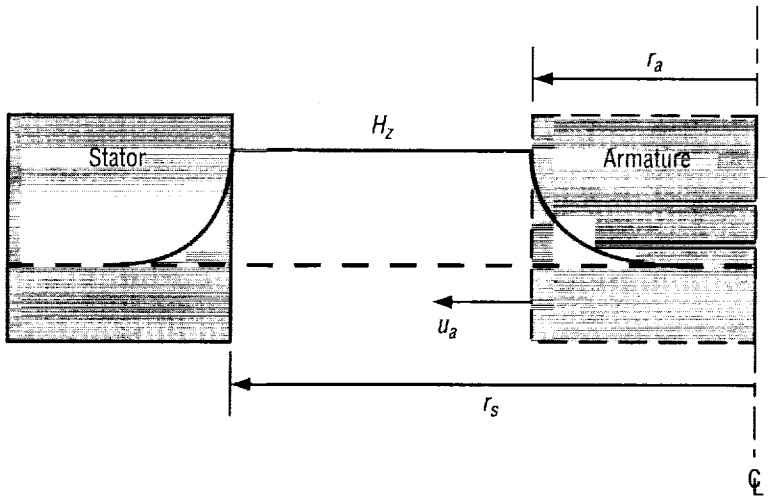

Figure 7. Illustration of magnetic diffusion processes in the stator and armature during field compression.

An expression for the instantaneous current is obtained from eq. (12) in the form:

$$\frac{i}{i_0} = \left(\frac{L_0}{L}\right)\lambda \quad . \tag{13}$$

The initial energy in the load is $W_0 = \frac{1}{2}L_0 i_0^2$ and the energy delivered to the load during field compression is $W_L = \frac{1}{2}L_L i^2$. Therefore, by taking the ratio of W_L to W_0 and substituting for i using eq. (13), the following expression is obtained:

$$\frac{W_L}{W_0} = \left(\frac{L_0}{L}\right)\left(\frac{L_L}{L}\right)\lambda^2 \quad . \tag{14}$$

The power delivered to the load P_L is defined by

$$P_L = \mathrm{V}_L i = \left(L_L \frac{di}{dt}\right) i \quad . \tag{15}$$

We note, however, that eq. (10) can be written as

$$\frac{di}{dt} = -i\left(R + \dot{L}_g\right)/L \quad , \tag{16}$$

and that $W_L = \frac{1}{2}L_L i^2$. Thus, the delivered power takes the form

$$P_L = -2W_L\left(R + \dot{L}_g\right)/L \quad . \tag{17}$$

The major point to note in the preceding circuit analysis is the impact of magnetic diffusion losses on generator performance. For example, the current multiplication ratio varies in proportion to λ ($i/i_0 \sim \lambda$), and the energy multiplication ratio varies in proportion to λ^2 ($W_L/W_0 \sim \lambda^2$). Therefore, if one hopes to achieve good reactor performance, it is essential that diffusion losses be minimized. This requires that both the stator and armature possess low magnetic diffusivity properties.

The fundamental definition of magnetic diffusivity in terms of material properties is

$$D_m = \frac{1}{\mu\sigma} \quad , \tag{18}$$

where μ is the magnetic permeability and σ is the electrical conductivity. Thus, it is desirable to utilize materials having the highest possible electrical conductivity.

3. MAGNETIC DIFFUSION ISSUES

The impact of magnetic diffusion losses is equally important to the performance of both propulsive and power reactors. The issues associated with stator and armature diffusion losses, including suitable design strategies, are discussed separately in sections 3.1 and 3.2.

3.1 Armature Concepts

The conventional approach in sacrificial magnetic flux compression reactors is to utilize a metal compression surface to minimize diffusion losses. In almost all cases, these designs incorporate a metal armature which is deformed and accelerated by high explosives. Magnetoimplosive generators, for instance, utilize this design principle with great success.

In principle, a target/cartridge is considered that is configured as a detonation charge surrounded by a thin metal liner, as illustrated in figure 8(a). However, the major drawbacks for the explosively driven metal liner approach are as follows: (1) The limited armature speed that can be achieved, (2) the likelihood of self-destruction which negates the desire for intermittent firing capability, and (3) general incompatibility with microfusion explosion schemes. For example, if one desires high-energy output (say 10^7 J) over a very short time interval (say 10 μsec) large-scale devices are required. This implies the need for a rapidly accelerated armature, a feat that is difficult to accomplish with existing technologies.

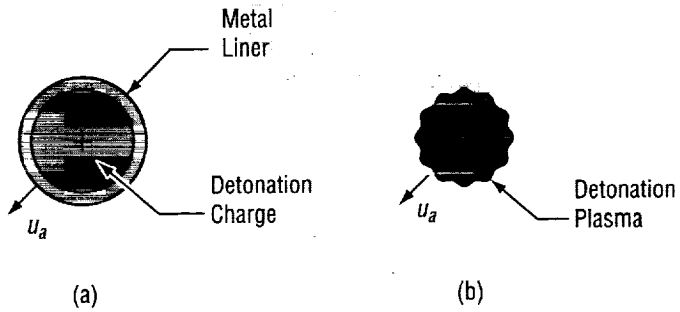

Figure 8. Illustration of explosively driven armatures:
(a) metal-lined cartridge and (b) detonation plasma.

An obvious solution to this dilemma is to attempt the use of a detonation plasma armature, as illustrated in figure 8(b). By eliminating the metal liner and relying on the intrinsic diamagnetic characteristics of the plasma cloud, it may be possible to obtain the desired field compression rate in an intermittently fired device. A comparison of metal versus plasma armature characteristics is shown in table 3.

Table 3. Metal versus plasma armature characteristics.

Parameter	Metal	Plasma
Conductivity	Very High	Relatively Low
Temperature	Very Low	Very High
Velocity	Very Low	Very High

The major advantages associated with the use of a plasma armature rather than a metal armature may be summarized as follows: (1) Greater speed (shorter pulse), (2) greater expansion/compression, (3) lower impulse delivered to reactor structure, (4) intermittent firing capability, (5) exhaust products can be readily utilized for propulsion, and (6) lower cost. These advantages are of special significance to space flight where simplicity and robust performance attributes are essential. On the other hand, plasma armatures introduce substantial technical risks that must be addressed and overcome through research and development.

The major technical risks/uncertainties associated with plasma armatures are as follows: (1) Achieving sufficiently high electrical conductivity to ensure diamagnetic behavior, (2) electron Joule heating effects, (3) field-aligned ion flow due to the ambipolar potential, (4) Rayleigh-Taylor surface instabilities, and (5) assurance of armature rebound.

The diamagnetic properties of the plasma armature can be quantitatively measured by the relative value of the magnetic Reynolds number, a parameter which naturally evolves from dimensional analysis of the magnetohydrodynamics (MHD) equations in the form

$$R_m = \frac{B_{ind}}{B_{app}} = \mu_0 \sigma_0 u_0 L_0 \quad , \tag{19}$$

where 0 subscript denotes an appropriate characteristic value for the problem. The plasma electrical conductivity is σ_0, u_0 is the plasma velocity, and L_0 is a characteristic length of the reactor (e.g., diameter). In a general sense, R_m may be thought of as a relative measure of the induced magnetic field in the plasma (B_{ind}) with respect to the external applied magnetic field (B_{app}). Because the magnetic Reynolds number is inversely related to the magnetic diffusivity D_m,

$$R_m = \frac{u_0 L_0}{D_m} \quad . \tag{20}$$

It is clear that for magnetic Reynolds numbers greater than unity, where the induced field is at least as strong as the applied field, the plasma will be resistive to magnetic diffusion. That is, the induced field associated with eddy currents in the plasma act in an opposing direction to the applied field, and if the induced field is high enough, the plasma interface effectively behaves as a magnetic compression surface.

The important point to note is that the magnetic Reynolds number depends primarily on the product σu such that one would desire high electrical conductivity and high expansion velocities in order to achieve low-flux diffusion losses. For fusion detonations, both of these parameters are extremely high and $R_m >> 1$, as desired. For conventional chemical detonations, the characteristic values are marginal and $R_m > 1$ can be achieved using carefully designed plasma-jet sources. It is believed that detonation plasmas using advanced HEDM materials may achieve $R_m > 1$, although this hope has yet to be demonstrated in the open literature.

3.2 Stator Concepts

The simplest approach to stator design is to utilize a metal having a high electrical conductivity, such as molydenum. In this way, one can satisfy the demands for both low magnetic diffusivity and high material strength in a relatively straightforward manner. Alternatively, possible utilization of a type II HTSC reaction chamber to confine the magnetic field as it is compressed outwardly by the expanding plasma is suggested. A type II HTSC stator, although prone to substantial technical risk, should be able to substantially reduce magnetic diffusion losses and significantly improve energy conversion efficiency.

Superconductors are divided into two types, depending on their characteristic behavior in the presence of a magnetic field. Type I superconductors comprised of pure metals tend to repel a penetrating magnetic flux due to the Meissner effect. In the Meissner state, the penetrating field is completely repelled from the interior of the superconductor.

For type I superconductors, the material is either perfectly conducting and exists in the Meissner state or it undergoes a phase transformation to the normal state. The major obstacle in using type I superconductors in a flux compression application is the low threshold values (i.e., temperature, current density, and magnetic field strength) defining critical transition to the normal state. The maximum critical field for a type I superconductor is $\approx$0.2 T, which is far too low for practical application in flux compression devices.

Ceramic-based type II superconductors, on the other hand, are potentially useful for flux compression applications due to the high critical threshold values which can be obtained. For example, the critical temperature is above liquid nitrogen temperatures over a wide range of current densities, and superconductivity can persist under applied magnetic fields exceeding 100 T.

In a type II superconductor, however, there are two critical field levels. The first critical field ($B_{c,1}$) defines the limiting value for maintaining a true Meissner state and is normally very small. When the applied field exceeds $B_{c,1}$, the material enters the so-called mixed state where the field penetrates in quantized amounts of flux. These points of penetration, known as fluxoids, may be envisioned as circulating vortices of current. The second critical field level ($B_{c,2}$) defines the transition to the normal state, and it can be large enough for practical flux compression application. Flux penetration in both the Meissner state and the mixed state as well as the characteristic variation of the critical fields for a type II HTSC are illustrated schematically in figure 9.

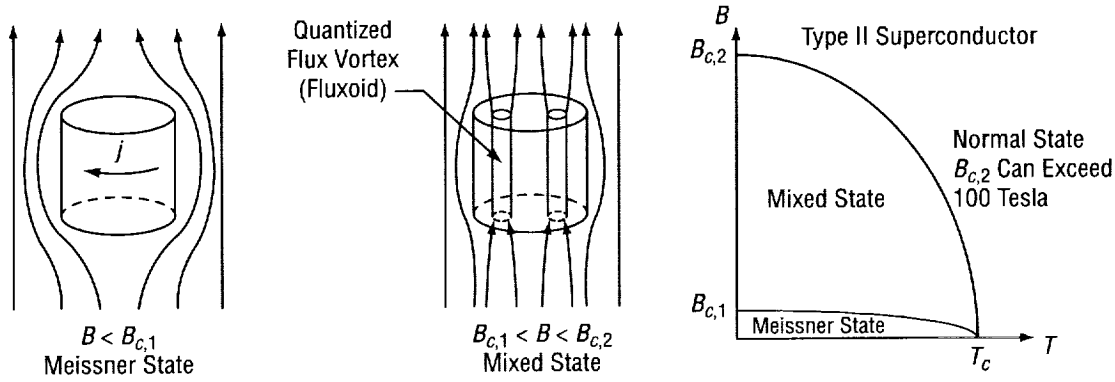

Figure 9. Illustration of superconductor field penetration in the Meissner state and the mixed state. Characteristic variation of the critical fields for a type II HTSC.

The interaction of the fluxoids with defects in the superconductor alters its conductive properties; that is, a fluxoid encompassing or adjacent to a defect has its energy altered and its free motion through the superconductor inhibited. This phenomenon, known as flux pinning, causes a field gradient in the superconductor and gives rise to a net current in the material. Since the pinning force is small, fluxoids can be broken loose from their pinning centers, resulting in a net creep of the flux through the conductor as a function of time. This results in an effective voltage in a type II superconductor.

If the current density is low and the magnetic field is not intense, flux creep is insignificant and the induced voltage and effective resistance will be essentially zero. At very high fields and high current densities, fluxoids will migrate rapidly, giving rise to a phenomenon called flux flow. The effective resistance can be non-negligible in the flux flow case, and breakdown to the normal state can ensue. This can be a particularly exacerbating issue when the flux skin depth is small and the induced current is high; because under these circumstances, the current density can be very high and may exceed the critical value for the HTSC.

Note that the magnetic diffusivity of a type II superconductor can be several orders of magnitude below that of the best metals, even in flux flow mode. For instance, recent studies investigating the magnetic diffusivity characteristics of various superconductor materials under pulsed magnetic fields indicate that the diffusivity can range from 10^{-2} to 10^{-6} m^2/sec.[29,30] This range can be compared with nominal values for various metals as indicated in table 4.

Table 4. Electrical and magnetic diffusivity properties of common metals.

Parameter	Dimension	Copper	Brass	Aluminum	Stainless Steel
ρ_0 (20 °C)	$\mu\Omega \cdot cm$	1.7	6.2	2.8	72
σ_0 (20 °C)	$10^6\ (\Omega \cdot m)^{-1}$	63.3	15.7	39.2	1.38
$D_m=(\mu_0\sigma_0)^{-1}$	m^2/sec	1.26	5.10	2.04	58

It is clear that for a type II HTSC, flux penetration will occur under an intense pulsed magnetic field. Therefore, some of the major questions that need to be answered are as follows: (1) How resistant are HTSC materials to magnetic field penetration in the mixed state? (2) How good are the magnetic diffusion characteristics in the mixed state? and (3) How does the HTSC material behave under intense applied-pulse fields, and will it break down?

The hope is that the transient magnetic field will exhibit a penetration time longer than the characteristic pulse time of the armature expansion process. This concept is illustrated schematically in figure 10 where a section of the HTSC stator wall is shown with an increasing magnetic field H inside a radial-mode reactor. The anticipated magnetic field profiles in the stator wall are shown at various instances in time during the armature expansion process. Note that there is some characteristic time (Δt_p) defining the penetration time of the magnetic field through the stator and some characteristic time defining the expansion time of the detonation plasma (τ_D). For practical purposes, it is necessary that $\Delta t_p > \tau_D$.

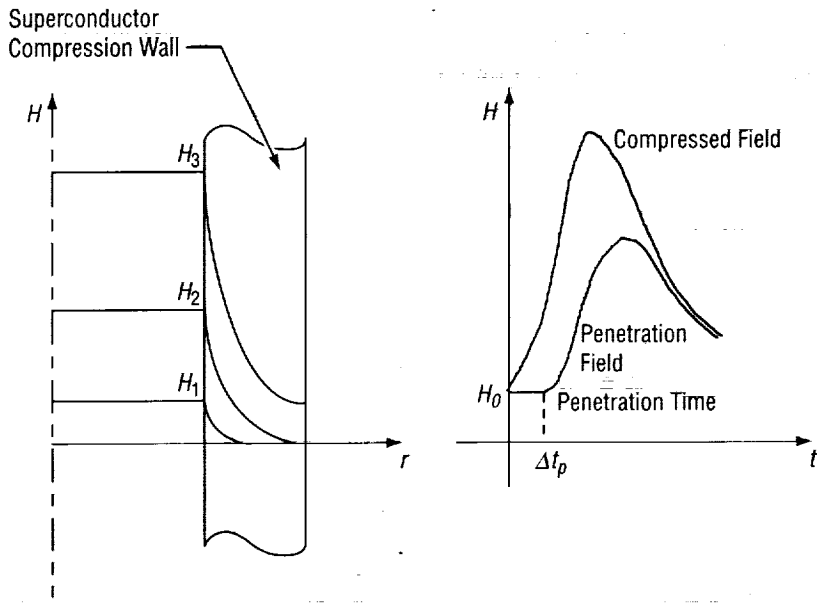

Figure 10. Illustration of transient magnetic field diffusion and penetration through an HTSC stator.

The HTSC stator concept is entirely hypothetical at this point and there are a whole host of significant research issues that must be addressed prior to practical implementation. The major uncertainties may be categorized as follows: (1) Breakdown of HTSC under strong pulsed fields, (2) hysteresis cycling of magnetization, (3) Joule/neutron heating of the material, (4) structural integrity under cyclic loading, and (5) bulk processed versus wire fabrication.

4. FLUX COMPRESSION DYNAMICS

Accurate analysis of the reactor requires formal solution of the MHD equations; however, it is instructive to develop a simplified analytical model for describing the dynamics of flux compression. This approach is adopted here, and a simple model for the radial-mode reactor developed (illustrated in fig. 4). This analysis includes finite conductivity effects and attempts to quantify flux diffusion losses and armature rebound criteria. The modeling approach is described in sections 4.1 through 4.4.

4.1 Field Amplification

During the explosive expansion of the plasma armature, some fraction of the trapped magnetic flux will diffuse into the armature and the stator. The flux which escapes from the annular containment region is lost for further compression and represents an inefficiency in generator performance. The field amplification, including losses, may be expressed in terms of the flux coefficient as defined in eq. (12):

$$\lambda = \frac{\phi}{\phi_0} = \frac{B\left(\pi r_s^2 - \pi r_a^2\right)}{B_0\left(\pi r_s^2 - \pi r_i^2\right)} = \frac{H\left(r_s^2 - r_a^2\right)}{H_0\left(r_s^2 - r_i^2\right)} \tag{21}$$

or

$$\frac{H}{H_0} = \lambda \frac{\left(r_s^2 - r_i^2\right)}{\left(r_s^2 - r_a^2\right)} , \tag{22}$$

where r_s is the internal radius of the magnetic flux containment stator, $r_i << r_s$ is the initial radius of the armature, and $r_a(t)$ is the time-dependent radius of the plasma armature.

Differentiation of eq. (22) yields

$$\frac{1}{H_0}\frac{dH}{dt} = 2\lambda u_a \frac{r_a\left(r_s^2 - r_i^2\right)}{\left(r_s^2 - r_a^2\right)^2} + \left(\frac{r_s^2 - r_i^2}{r_s^2 - r_a^2}\right)\frac{d\lambda}{dt} , \tag{23}$$

where $u_a = dr_a / dt$. Using eq. (22), the following is obtained:

$$\frac{1}{H_0}\frac{dH}{dt} = 2\lambda u_a \frac{H}{H_0}\frac{1}{\lambda}\frac{r_a}{\left(r_s^2 - r_a^2\right)} + \frac{H}{H_0}\frac{1}{\lambda}\left|\frac{d\lambda}{dt}\right| \tag{24}$$

or

$$\frac{1}{H}\frac{dH}{dt} = \frac{2r_a}{r_s^2 - r_a^2}u_a - \frac{1}{\lambda}\left|\frac{d\lambda}{dt}\right| \ . \tag{25}$$

This result demonstrates that the maximum field amplification can occur during armature expansion and not necessarily when $u_a \rightarrow 0$.

An alternative form for field amplification can be developed through the introduction of the flux skin depth, which defines the flux penetration depth during the compression process. The concept of flux skin depth is illustrated in figure 11. The flux skin depth is defined by taking the magnetic field at the surface as an effective constant value and requiring that the flux contained within a skin depth, s_ϕ, be equivalent to the total diffused flux. Conserving the total flux (contained and leakage),

$$\mu H_0 \pi\left(r_s^2 - r_i^2\right) = \mu H \pi\left[\left(r_s + s_{\phi,s}\right)^2 - \left(r_a - s_{\phi,a}\right)^2\right] \ , \tag{26}$$

yielding

$$\frac{H}{H_0} = \frac{\left(r_s^2 - r_i^2\right)}{\left(r_s + s_{\phi,s}\right)^2 - \left(r_a + s_{\phi,a}\right)^2} \ . \tag{27}$$

Combining eqs. (22) and (27) gives an expression for λ in terms of the flux skin depths in both the armature and stator:

$$\lambda = \frac{\phi}{\phi_0} = \frac{\left(r_s^2 - r_a^2\right)}{\left(r_s - s_{\phi,s}\right)^2 - \left(r_a - s_{\phi,a}\right)^2} \ . \tag{28}$$

For a reasonable estimation of the compression dynamics, it is generally sufficient to use appropriate approximations or analytical solutions for s_ϕ. This approach is known as the skin layer method in which it is assumed that the flux loss and penetration velocity of the diffused magnetic field remain limited. That is, $s_\phi << (r_s - r_a)$, $ds_\phi/dt << u_a$, $s_{\phi,a} << r_a$, and $s_{\phi,s} << d$ where d is the thickness of the stator.

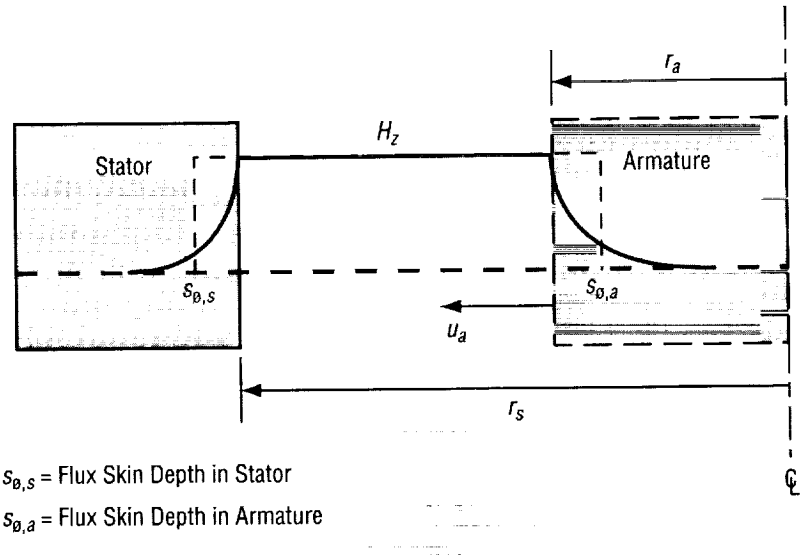

Figure 11. Illustration of flux skin depth concept as applied to flux compression reactor geometry.

4.2 Flux Skin Depth in Planar Geometry

To determine the time-varying flux skin depth in a semi-infinite planar geometry, the magnetic diffusion equation is solved assuming an exponentially increasing magnetic field $H/H_0 = \chi(t) = \exp t/\tau_c$ where τ_c is the characteristic time for magnetic compression and is associated with the plasma expansion speed. The planar geometry approximation can be invoked whenever flux skin depth is smaller than the radius of curvature.

The magnetic diffusion equation for a semi-infinite planar one-dimensional (distance and time as independent variables) geometry with a magnetic field oriented perpendicular to the surface has the form

$$\frac{1}{D_m}\frac{\partial H}{\partial t} + \frac{\partial^2 H}{\partial \varsigma^2} = 0 \quad , \tag{29}$$

where the following stationary boundary condition applies

$$H(0,t) = H_0 e^{t/\tau_c} \quad ; \quad -\infty < t < \infty \quad . \tag{30}$$

By seeking a solution of the form $\exp t/\tau_c f(x)$, a differential equation for f is obtained as

$$\frac{\partial^2 f}{\partial \varsigma^2} = \frac{f}{D_m \tau_c} \tag{31}$$

from which following the general solution is deduced:

$$H(\varsigma,t) = H_0 e^{t/\tau_c}\left(A_1 e^{-\varsigma/\varsigma_0} + A_2 e^{\varsigma/\varsigma_0}\right) , \tag{32}$$

where

$$\varsigma_0 = \sqrt{D_m \tau_c} \quad . \tag{33}$$

The only physically acceptable solution, which satisfies the requirement for a monotonically decreasing field in the conductor, is

$$H(\varsigma,t) = H_0 \exp\left(\frac{t}{\tau_c} - \frac{\varsigma}{\varsigma_0}\right) . \tag{34}$$

Again, the flux skin depth is defined such that the diffused flux $\phi_{diff}(t)$ into the surface can be expressed by the surface flux density $B_{surf}(t)$ spread over a depth s_ϕ:

$$\phi_{diff}(\tau) = B_{surf}(t) s_\phi = \int_0^\infty B(\varsigma,\tau) d\varsigma \tag{35}$$

or

$$H_{surf}(t) s_\phi = \int_0^\infty H(\varsigma,\tau) d\varsigma \quad . \tag{36}$$

Thus, evaluation of the integral using the profile defined by eq. (34) yields the desired expression for the flux skin depth

$$s_\phi = \varsigma_0 = \sqrt{D_m \tau_c} \quad . \tag{37}$$

4.3 Skin Layer Methodology

A simple estimation of flux efficiency may be obtained using Sakharov's skin layer methodology.[31] Although the electrical conductivity will depend on a number of factors which vary during the course of compression, consideration is limited to the case of finite and constant electrical conductivity in order to avoid the need to solve a system of partial differential equations. The physical motivation for the skin layer methodology is based on the fact that the skin layer depth is dominated by the ever-increasing field so that the contribution from the previous initial condition is rapidly lost.

In the skin layer methodology, the distribution of current in the compression surfaces is approximated by an exponential profile:

$$j_s = j_{0,s} e^{-\zeta / s_{\phi,s}} \quad \text{and} \quad j_a = j_{0,a} e^{-\zeta / s_{\phi,a}} \ . \tag{38}$$

These relationships are exact if H increases exponentially on the boundary; i.e., $H/H_0 = \exp t/\tau_c$. It is clear that the following differential relationship must then hold true:

$$\frac{dH}{dt} = \frac{H}{\tau_c} \ . \tag{39}$$

Introducing eq. (25), the following is obtained:

$$\tau_c = \frac{H}{dH/dt} = \left[\left(\frac{2r_a}{r_s^2 - r_a^2} \right) u_a - \frac{1}{\lambda} \left| \frac{d\lambda}{dt} \right| \right]^{-1} \ . \tag{40}$$

Assuming the change in flux as a correction factor ($d\lambda/dt << 1$; $\lambda \sim 1$), the following approximation is arrived at for the time-dependent variation in τ_c:

$$\tau_c = \frac{H}{dH/dt} \approx \frac{r_s^2 - r_a^2}{2 r_a u_a} \ . \tag{41}$$

This approximation implicitly assumes that the flux loss and penetration velocity of the differential fields remain limited (i.e., $s_\phi << r_s - r_a$ and $ds_\phi/dt << u_a$).

With reference to figures 4 and 6, Farady's law is applied to the stator and armature to obtain

$$\oint_{C_s} \mathbf{E}_s \cdot d\mathbf{l} = \frac{d\phi}{dt} + \frac{d\phi_a}{dt} \tag{42}$$

$$\oint_{C_a} \mathbf{E}_a \cdot d\mathbf{l} = \frac{d\phi_a}{dt} \ , \tag{43}$$

where $\phi = \phi_0 - \phi_s - \phi_a$ is the trapped flux. Combining eqs. (42) and (43) yields

$$\oint_{C_s} \mathbf{E}_a \cdot d\mathbf{l} - \oint_{C_a} \mathbf{E}_a \cdot d\mathbf{l} = \frac{d\phi}{dt} \tag{44}$$

or

$$2\pi r_s E_s^* + 2\pi r_a E_a^* = \frac{d\phi}{dt} \ , \tag{45}$$

where it was taken into account the fact that $\mathbf{E}_s$ and $\mathbf{E}_a$ are in opposing directions due to Lenz's law. $\mathbf{E}^*=\mathbf{E}+(\mathbf{u}\times\mathbf{B})$ is the electric field detected by an observer moving with the medium. Therefore,

$$E_s^* = \frac{j_{0,s}}{\sigma_s} \quad \text{and} \quad E_a^* = \frac{j_{0,a}}{\sigma_a} \tag{46}$$

and eq. (45) may be written as

$$2\pi r_s \frac{j_{0,s}}{\sigma_s} + 2\pi r_a \frac{j_{0,a}}{\sigma_a} = \frac{d\phi}{dt} \ . \tag{47}$$

Now, Maxwell's equations require that $\nabla\times\mathbf{H}=0$ at the compression surfaces such that

$$-\frac{\partial H}{\partial \zeta} = j \ . \tag{48}$$

Using the assumed current density distribution ($j=j_0\exp-\zeta/s_\phi$) in eq. (48) yields the differential relationship:

$$-\frac{dH}{d\zeta} = j_0 e^{-\zeta/s_\phi} \ . \tag{49}$$

Separating variables and integrating,

$$dH = -j_0 \int_0^\infty e^{-\zeta/s_\phi} d\zeta \tag{50}$$

$$H = -j_0 s_\phi \left[e^{-\zeta/s_\phi} \right]_0^\infty = j_0 s_\phi \ . \tag{51}$$

Therefore, eq. (47) may be written in the form

$$\frac{d\phi}{dt} = \frac{2\pi r_s H}{\sigma_s s_{\phi,s}} + \frac{2\pi r_a H}{\sigma_a s_{\phi,a}} \ . \tag{52}$$

By definition, the trapped flux is given by

$$\phi = \mu H \pi \left(r_s^2 - r_a^2 \right) \tag{53}$$

and eq. (52) becomes

$$\frac{d\phi}{dt} = \left(\frac{r_s}{\sigma_s s_{\phi,s}} + \frac{r_a}{\sigma_a s_{\phi,a}} \right) \frac{2\phi}{\mu\left(r_s^2 - r_a^2\right)} \quad . \tag{54}$$

Defining $dr_a/dt = -u_a$ such that $dt = -dr_a/u_a$ where u_a is the velocity of the expanding armature, substituting into eq. (54), and separating variables yields

$$-\frac{d\phi}{\phi} = \left(\frac{r_s}{\mu\sigma_s s_{\phi,s}} + \frac{r_a}{\mu\sigma_a s_{\phi,a}} \right) \frac{2dr_a}{u_a\left(r_s^2 - r_a^2\right)} \quad . \tag{55}$$

For a reasonable estimation of compression dynamics accounting for magnetic diffusion losses, the flux skin depth approximation is applied for a semi-infinite planar geometry to both the stator and armature. Then, eq. (55) takes the following form:

$$-\frac{d\phi}{\phi} = \left(\frac{r_s}{\mu\sigma_s\sqrt{D_{m,s}\tau_c}} + \frac{r_a}{\mu\sigma_a\sqrt{D_{m,a}\tau_c}} \right) \frac{2dr_a}{u_a\left(r_s^2 - r_a^2\right)} \quad . \tag{56}$$

Regarding the change in flux as a correction, the time-dependent relationship is utilized for τ_c as defined by eq. (41) such that eq. (56) becomes

$$-\frac{d\phi}{\phi} = \left[r_s\sqrt{\frac{D_{m,s}}{u_a}} + r_a\sqrt{\frac{r_s}{R_{m,a}}} \right] \frac{2\sqrt{2r_a}dr_a}{\left(r_s^2 - r_a^2\right)^{3/2}} \quad , \tag{57}$$

where the magnetic Reynolds number is defined for the armature as $R_{m,a} = \mu\sigma_a u_a r_s$.

It is convenient at this point to nondimensionalize the problem in terms of a flux compression coefficient λ and a dimensionless independent variable ξ:

$$\lambda = \phi/\phi_0 \quad \Rightarrow \quad \phi_0 d\lambda = d\phi \tag{58}$$

$$\xi = r_a/r_s \quad \Rightarrow \quad r_s d\xi = dr_a \quad . \tag{59}$$

Therefore, eq. (56) takes the desired final form

$$-\frac{d\lambda}{\lambda}=\left[\sqrt{\frac{D_{m,s}}{u_a}}+\xi\sqrt{\frac{r_s}{R_{m,a}}}\right]\frac{2\sqrt{2\xi}d\xi}{\sqrt{r_s}\left(1-\xi^2\right)^{3/2}} \quad . \tag{60}$$

This equation can be numerically integrated to determine the evolution of the flux coefficient λ as a function of the armature expansion ratio ξ.

4.4 Armature Rebound Condition

With appropriate design, the increasing magnetic pressure due to flux compression will decelerate the expanding plasma armature until it is completely stopped and the motion is reversed. If this rebound process does not occur, the plasma will impact the reaction chamber wall, most likely with disastrous results. Clearly, stator impact is incompatible with repetitive operation and an estimate of the turnaround distance is essential.

At the turnaround point, the assumption is made that the useful energy production per detonation has been transformed into magnetic energy. Thus,

$$W_{m,t}=W_{m,0}+\eta W_k \quad , \tag{61}$$

where $W_{m,t}$ is the magnetic field energy at the turnaround point

$$W_{m,t}=\left[\frac{1}{2}\mu H_t^2\right]V_t \quad , \tag{62}$$

and $W_{m,0}$ is the original magnetic field energy in the reaction chamber

$$W_{m,0}=\left[\frac{1}{2}\mu H_0^2\right]V_0 \quad , \tag{63}$$

W_k is the kinetic energy production per detonation, and η is the energy conversion efficiency with which the available detonation energy is transformed into a magnetic field energy. V_t and V_0 are the flux containment volumes at the turnaround point and at the beginning of armature expansion, respectively:

$$V_t=\pi\left[\left(r_s+s_{\phi,s}\right)^2-\left(r_i-s_{\phi,a}\right)^2\right]z \tag{64}$$

$$V_0=\pi\left[r_s^2-r_i^2\right]z \quad , \tag{65}$$

and z is the height of the reaction chamber. Furthermore, it is assumed that

$$W_k = w_D \rho_D \pi r_i^2 z \ , \tag{66}$$

where w_D is the detonation energy per unit mass. Dividing eq. (61) through by $W_{m,0}$ and evaluating eq. (27) at the turnaround point yields the following relationship:

$$\frac{H_t}{H_0} = \frac{\left(r_s^2 - r_i^2\right)}{\left(r_s + s_{\phi,s}\right)^2 - \left(r_t + s_{\phi,a}\right)^2} = 1 + \frac{\eta W_k}{W_{m,0}} \ . \tag{67}$$

The turnaround radius, r_t, is defined as the radial location at which eq. (67) is satisfied.

5. MARK I DEVICE

In the near term, it is anticipated that meaningful technology demonstration experiments could utilize high-explosive detonation charges in order to establish scientific feasibility, since microfusion and HEDM technologies are still several years away from fruition.

The chief difficulty encountered with high-explosive plasma jets is the limited magnetic Reynolds numbers that can be achieved. The detonation velocity of high-explosive plasma jets is typically on the order of 10^4 m/sec, and this level of performance can only be achieved through special shaped charge configurations.

Experimental investigations of shaped charge explosives as applied to MHD generator applications have been conducted in the past.[32] This included high-speed imaging of the plasma jet and measurement of its velocity and electrical conductivity. In these tests, it has been observed that a cohesive, hot, rosy-colored plasma slug is projected at speeds on the order of 3×10^4 m/sec. Figure 12 shows the measured electrical conductivity in a plasma jet from a 44° cavity charge of unseeded composition–4 (C4). Note that the measured conductivity in the slug exceeded 10^4 S/m. Inserting representative values for the jet velocity and electrical conductivity into the expression for the magnetic Reynolds number, as defined by eq. (19), and assuming a reasonable length scale for a practical device, it is found that

$$R_m = \mu_0\sigma_0 u_0 L_0 = 4\pi(10)^7(10)^4(10)^4(10)^{-1} > 1 \quad . \tag{68}$$

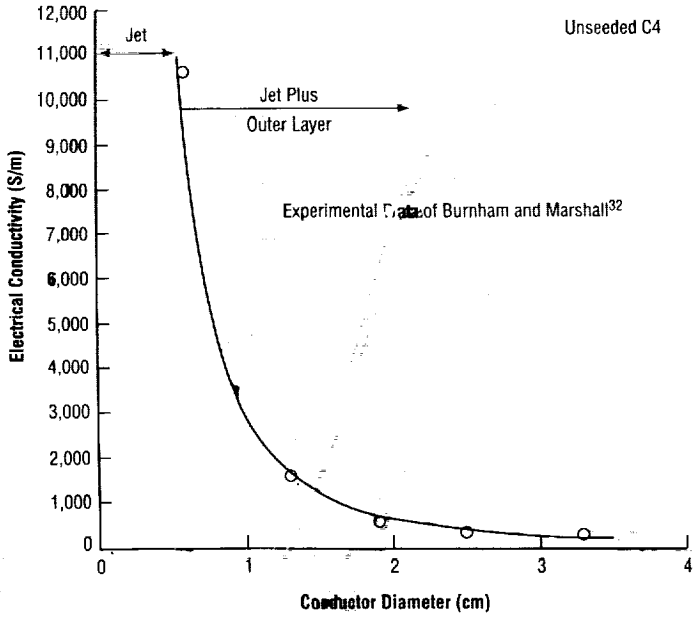

Figure 12. Measured electrical conductivity in a conical charge plasma jet of unseeded C4.

A practical demonstration device can be developed using a non-nuclear plasma source, based on these results. A demonstration device along the lines of the Mark I configuration depicted in figure 13 would be a logical step in this direction. This device is envisioned as a $^1/_2$-m-diameter reaction chamber, which uses colliding plasma jets from opposing high-explosive charges to produce a radially expanding armature. The formation of a radially expanding plasma jet from two colliding jets has been previously demonstrated on a small scale.[32] The observed collisional process in these experiments is illustrated in figure 14.

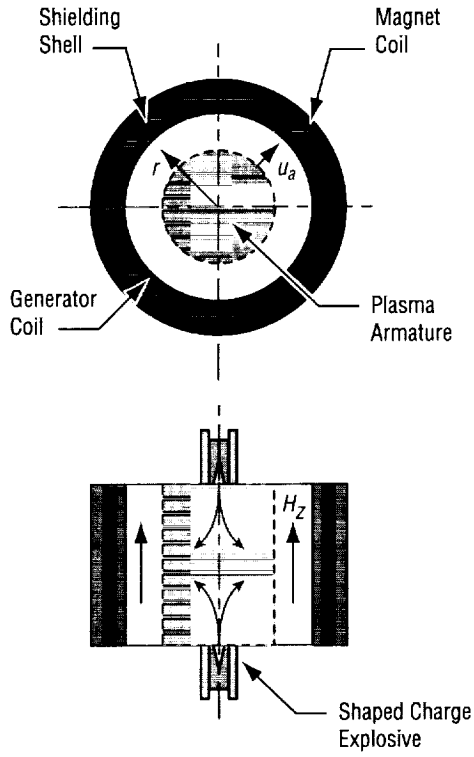

Figure 13. Mark I configuration for a radial-mode explosively driven demonstration device.

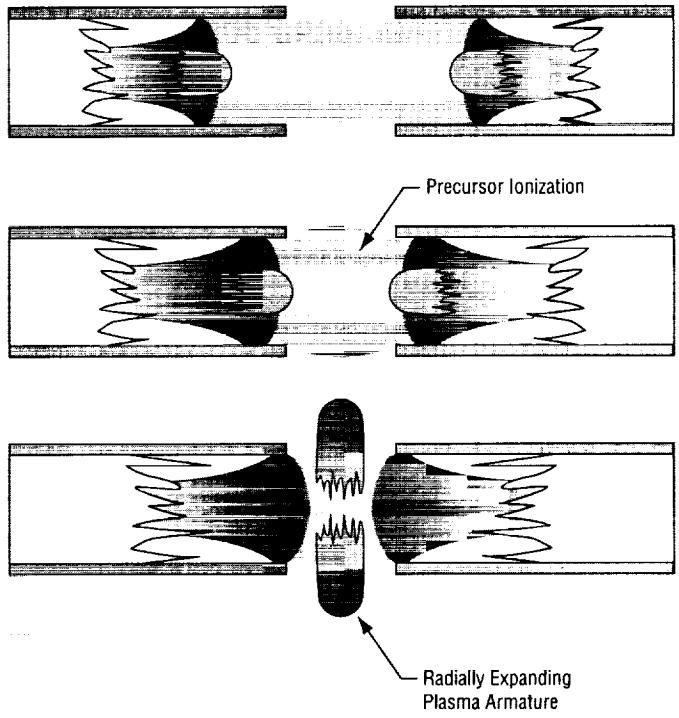

Figure 14. Illustration of plasma jet collisional process and radial armature formation.

5.1 Representative Calculations

As a precursor analysis to the Mark I configuration, calculations based on the skin layer methodology have been performed. The calculations presume an internal generator diameter of 0.5 m and various stator materials were investigated. Typical parameters for high-explosive detonations used in the calculations are summarized in table 5.

Table 5. High-explosive characteristics.

Density (ρ_D)	1,700 kg/m^3
Specific Energy (w_D)	5×10^6 J/kg
Velocity (u_D)	1×10^4 m/sec

The variation in the flux coefficient as a function of the armature expansion ratio is shown in figure 15. Numerical integration of eq. (60) was performed for magnetic Reynolds numbers of 1 and 10, assuming stator materials of steel, copper, and a hypothetical HTSC. For the hypothetical HTSC stator material, a magnetic diffusivity value of 10^{-5} m^2/sec was assumed. With a magnetic Reynolds number of unity, an increasing compression efficiency was observed as the material conductivity increases, although the result for HTSC is not as encouraging as desired. When the magnetic Reynolds number is increased to 10, a significant increase in compression efficiency was noted for all stator materials.

Calculations for the armature turnaround radius as a function of initial seed field were carried out for a copper stator assuming an energy conversion efficiency of 50 percent. The results are presented in figure 16 for various magnetic Reynolds numbers. There is a minimum initial seed field, the value of which depends on the magnitude of flux diffusion losses, to avoid stator impact. With a good stator material and high R_m, it is possible to reduce the seed field and minimize system size and weight.

Apparently, significant flux compression can be accomplished at marginal magnetic Reynolds numbers when the stator material is sufficiently resistant to magnetic diffusion. Thus, it appears that a successful demonstration device could be developed, which utilizes a non-nuclear high-explosive plasma jet source. The preceding analysis is highly idealized, of course, and real hydrodynamic effects will lead to more pessimistic predictions with respect to the minimum required magnetic Reynolds number; however, the simplified analysis results appear encouraging.

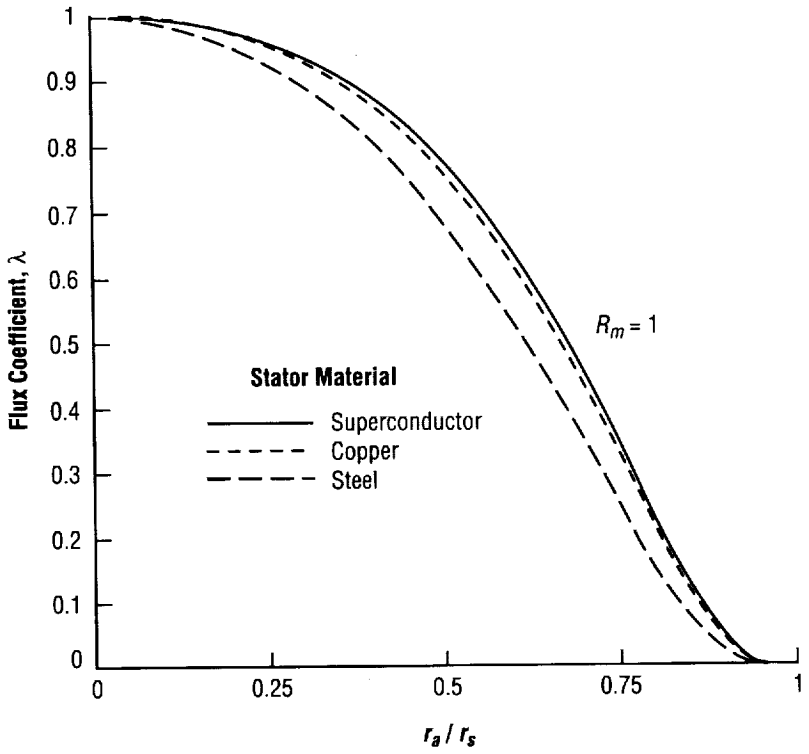

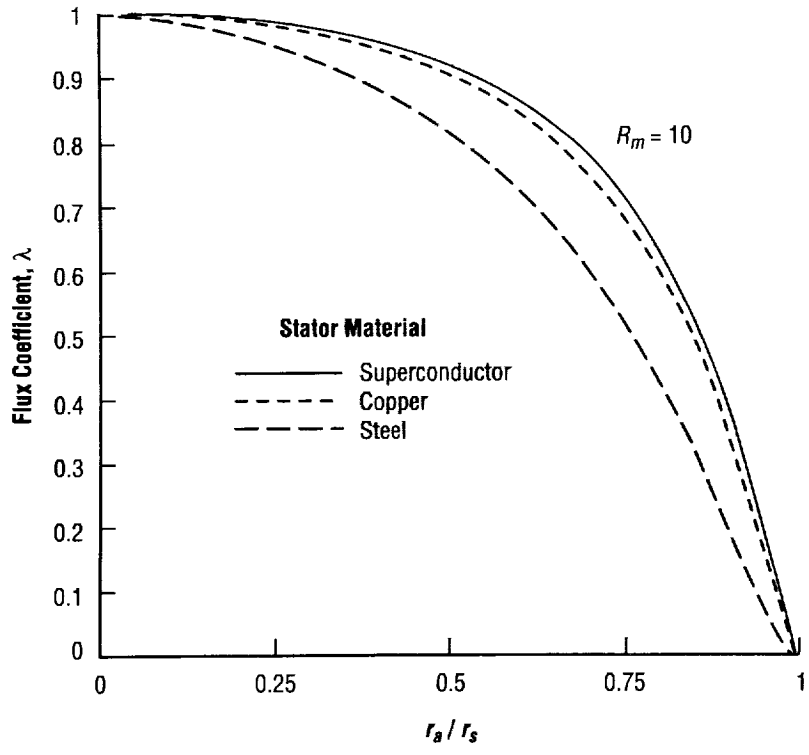

Figure 15. Computed flux coefficient for Mark I.

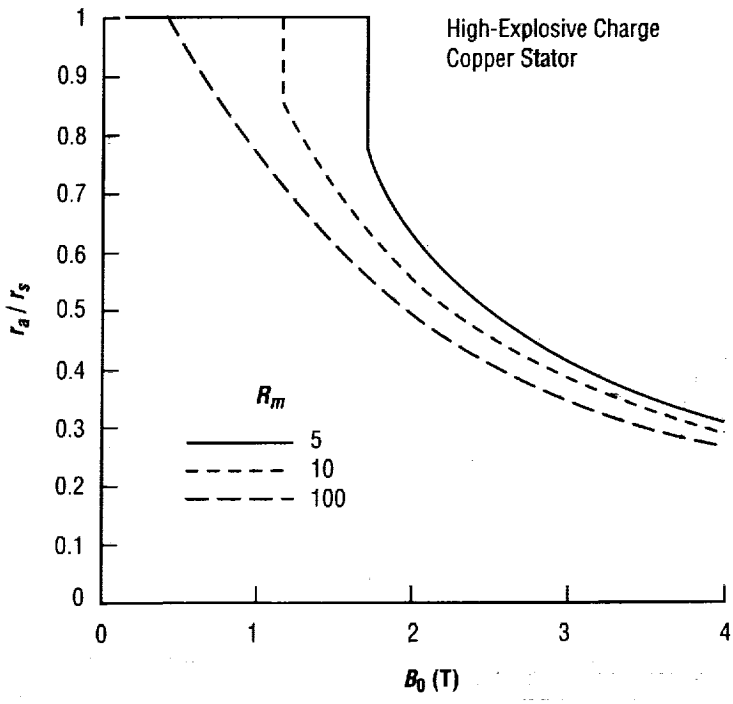

Figure 16. Computed armature rebound radius.

6. MAGNETIC DIFFUSION LABORATORY EXPERIMENTS

6.1 Analytical Model

As part of this research, simple laboratory experiments were designed to investigate the magnetic diffusivity characteristics of HTSC samples when exposed to strong-pulsed magnetic fields. The basic configuration in these experiments, as illustrated in figure 17, is a hollow tube of test material surrounded by a solenoid, which can be used to create a pulsed external magnetic field on demand. Measurement of the time-varying magnetic field inside the tube, once the solenoid is pulsed, yields quantitative information with respect to the magnetic diffusivity properties of the material. In sections 6.1 and 6.2, an analytical treatment of the magnetic diffusion process through a conducting hollow cylinder is described and the preliminary experimental results discussed.

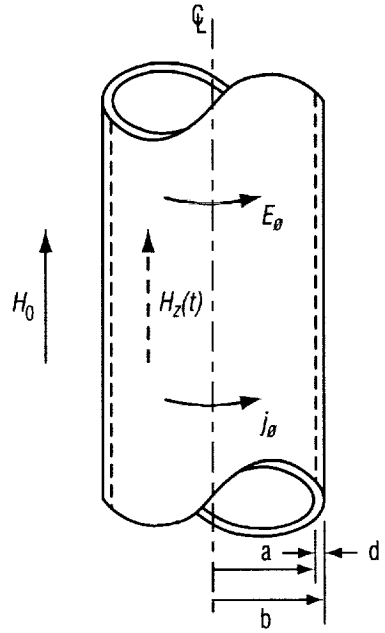

Figure 17. Illustration of experimental configuration for examining pulsed magnetic diffusion through a hollow conducting cylinder.

The magnetic diffusion through a conducting hollow cylinder is governed by a magnetic diffusion equation derived from Maxwell's electromagnetic laws. In a cylindrical coordinate system, the governing diffusion equation has the form[33]

$$\frac{\partial^2 H}{\partial r^2} + \frac{1}{r}\frac{\partial H_z}{\partial r} = \frac{1}{D_m}\frac{\partial H_z}{\partial t} \quad , \tag{69}$$

and the following initial/boundary conditions apply:[33]

$$H_z(b,t) = H_0 \tag{70}$$

$$H_z(r,0) = 0 \tag{71}$$

$$\left.\frac{dH_z}{dt}\right|_a = \frac{2D_m}{a}\left[\frac{\partial H_z}{\partial r}\right]_{r=a} . \tag{72}$$

The solution to this system of equations is known from mathematical physics using the Laplace transform methodology. The field $H_z(t) = H_z(a,t)$, which is built up in the cavity of the conductor, can be given for $\mu_R = 1$ in the form[33]

$$H_z(a,t) = H_0 - 4H_0 \sum_{n=1}^{\infty} e^{-D_m \alpha_n^2 t} \left\{ \frac{J_2(a\alpha_n) J_0(b\alpha_n)}{(a\alpha_n)^2 \left[J_0^2(b\alpha_n) - J_2^2(a\alpha_n) \right]} \right\} , \tag{73}$$

where the α_n are roots of

$$J_0(b\alpha) Y_2(a\alpha) - Y_0(b\alpha) J_2(a\alpha) = 0 \tag{74}$$

and J_n and Y_n are Bessel functions of the first and second kind of order n, respectively.

After a long enough time, such that

$$t \geq \frac{1}{D_m \alpha_1^2} , \tag{75}$$

it is sufficient to retain only the first ($n = 1$) term. The field growth in the conductor is then

$$H_z(a,t) \approx H_0 \left(1 - e^{-t/\tau_1}\right) , \tag{76}$$

where

$$\tau_1 = \frac{1}{D_m \alpha_1^2} = \frac{b^2}{4\pi D_m} g . \tag{77}$$

The parameter g, defined by

$$g = \frac{4\pi}{(b\alpha_1)^2} \quad , \tag{78}$$

is a geometrical form factor which has been tabulated as a function of the ratio a/b in table 6.[34]

Table 6. Tabulation of geometric form factor as a function of the tube radius ratio.

a/b	g	a/b	g
0.00	2.173	0.65	1.587
0.05	2.173	0.70	1.431
0.10	2.172	0.75	1.253
0.15	2.170	0.80	1.052
0.20	2.164	0.85	0.8267
0.25	2.153	0.90	0.5766
0.30	2.133	0.95	0.3011
0.35	2.102	0.96	0.2430
0.40	2.059	0.97	0.1838
0.45	2.001	0.98	0.1236
0.50	1.926	0.99	0.0623
0.55	1.833	1.00	–
0.60	1.720		

In our small-scale experiments, the tube size was as follows: length = 75 mm, wall thickness = 7.14375 mm, and outside diameter = 30.1626 mm. This yields an inner radius of $a = 0.079375$ cm and an outer radius of $b = 1.508125$ cm. Thus, $g = 1.8771$ (from table 6) and the characteristic diffusion time may be estimated according to eq. (77). The characteristic diffusion times, assuming a range of conductivity values for the HTSC material, are summarized in figure 18. Actual diffusion characteristics of the HTSC material will depend on the behavior of the superconductor under strong pulsed fields. Based on the experimental efforts of previous researchers, D_m is anticipated to fall in the range of 10^{-5} to 10^{-3} m^2/sec.

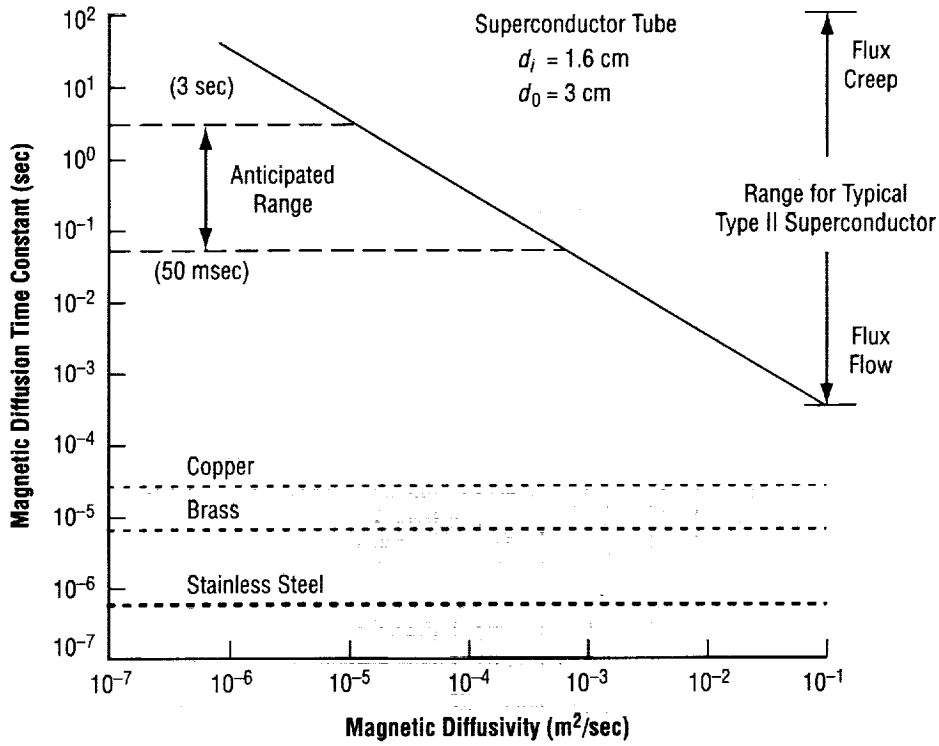

Figure 18. Characteristic magnetic diffusion time constant for magnetic field penetration through conducting hollow cylinders of various materials with $g = 1.8771$.

6.2 Laboratory Experiments

The objective of the experiments was to measure the magnetic diffusion rate of $Bi_2Sr_2CaCu_2O_x$ (BSCCO) superconducting material in comparison with conventional metals.

The experimental apparatus consists of a cylindrical tube surrounded by an excitation coil. A Hall probe is placed along the centerline of the tube to measure the instantaneous magnetic field, and a Rogowski coil is looped around the tube and coil as a means of measuring the induced current. The entire test section is submerged in liquid nitrogen for testing. Different materials (i.e., copper, aluminum, and steel) were tested in order to compare their magnetic diffusion rates to that of the superconductor.

During testing, it can be expected that a time delay will occur between the external excitation field and internal field shielded by the tube. From this experimentally measured time delay, the magnetic diffusion characteristics of the material can be deduced.

Some typical results from these experiments are provided in figure 19 for aluminum and BSCCO materials. These results indicate a time delay of ≈45 msec for BSCCO which may be compared with a time delay of 4 msec for aluminum. Although preliminary in nature, these data indicate a significant improvement in penetration delay time and are sufficiently encouraging to warrant further investigation.

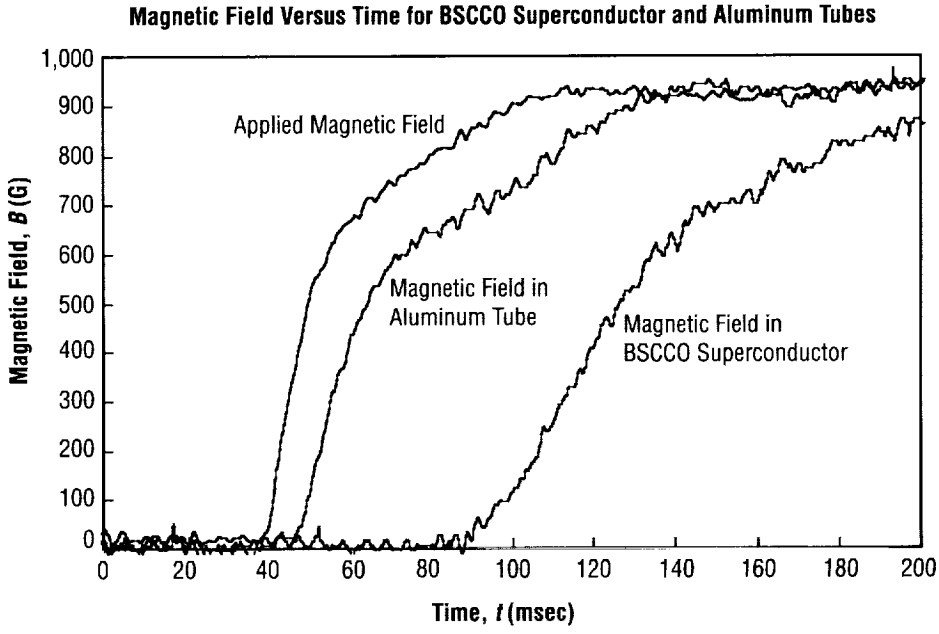

Figure 19. Magnetic penetration time delay characteristics for BSCCO and aluminum tubes.

7. CONCLUSIONS

Magnetic flux compression reactors are technically feasible for spacecraft propulsion and power, based on our preliminary assessment. It appears that high-power density systems can be designed which can utilize a detonation plasma armature in conjunction with a highly conductive stationary stator. In this way, one could develop an intermittently fired reactor using microfusion or advanced HEDM targets for the direct production of electrical power and thrust.

A Mark I demonstration radial-mode reactor driven by chemical high explosive is also proposed. Analyses of the conductivity and velocity produced by shaped charge plasma jets indicate that one can achieve $R_m > 1$ using non-nuclear sources. A skin layer analysis of the concept indicates that effective flux compression can be achieved in a relatively moderate scale device. In addition, the potential for improved field compression using type II HTSC stator materials was evaluated, but the performance gains were marginal based on the assumed conductivity value. Small-scale laboratory experiments did show that BSCCO has a significantly lower magnetic diffusivity in comparison to conventional metals, but further research is needed to clarify the actual system-level benefits. The major technical issues associated with the use of a plasma armature appear to be achieving good diamagnetic properties and controlling Rayleigh-Taylor surface instabilities.

REFERENCES

1. Winterberg, F.: "Rocket Propulsion by Thermonuclear Microbombs Ignited With Intense Relativistic Electron Beams," *Raumfahrt-forschung*, Vol. 15, pp. 208–217, 1971.

2. Hyde, R.A.; Wood, Jr., L.L.; and Nuckolls, J.H.: "Prospects for Rocket Propulsion With Laser-Induced Fusion Microexplosions," *AIAA Paper 72–1063*, 1972.

3. Hyde, R.; Wood, L.; and Nuckolls, J.: "Propulsion Applications of Laser-Induced Fusion Microexplosions," *Proc. of the First Topical Mtg. Technology of Controlled Nuclear Fusion*, G.R. Hopkins (ed.), Report CONF–740402-P1, U.S. Atomic Energy Commission, pp. 159–164, 1974.

4. Winterberg, F.: "Rocket Propulsion by Staged Thermonuclear Microexplosions," *Journal of the British Interplanetary Society*, Vol. 30, pp. 333–340, 1977.

5. Martin, A.R.; and Bond, A.: "Nuclear Pulse Propulsion: A Historical Review for an Advanced Propulsion Concept," *Journal of the British Interplanetary Society*, Vol. 32, pp. 283–310, 1979.

6. Martin, A.R.; and Bond, A.: "Project Daedalus: The Propulsion System; Part I: Theoretical Considerations and Calculations," in *Project Daedalus—Final Report on the the BIS Starship Study*, A.R. Martin (ed.), *Journal of the British Interplanetary Society*, pp. S44–S61, 1978.

7. Bond, A.; and Martin, A.R.: "Project Daedalus: The Propulsion System; Part II: Engineering Design Considerations and Calculations," in *Project Daedalus—Final Report on the BIS Starship Study*, A.R. Martin (ed.), *Journal of the British Interplanetary Society*, pp. S63–S82, 1978.

8. Winterberg, F.: "Rocket Propulsion by Nuclear Microexplosions and the Interstellar Paradox," *Journal of the British Interplanetary Society*, Vol. 32, pp. 403–409, 1979.

9. Reupke, W.A.: "Implications of Inertial Fusion Systems Studies for Rocket Propulsion," *AIAA Paper 82–1213*, 1982.

10. Hyde, R.A.: "A Laser Fusion Rocket for Interplanetary Propulsion," *IAF–83–396*, 1983.

11. Borowski, S.K.: "Comparison of Fusion/Anitiproton Propulsion Systems for Interplanetary Travel," *NASA TM–107030* (*AIAA Paper 87–1814*), 1987.

12. Orth, C.; Klein, G.; Sercel, J.; Hoffman, N.; Murray, K.; and Chiang-Diaz, F.: "Transport Vehicle for Manned Mars Missions Powered by Inertial Confinement Fusion," *AIAA Paper 87–1904*, 1987.

13. Orth, C.D.: "Interplanetary Space Transport Using Inertial Fusion Propulsion," *Proc. Ninth Int. Conf. on Emerging Nuclear Energy Systems (ICENES '98; Herzliya, Israel)*, Vol. 1, pp. 253–263, 1998.

14. Shmatov, M.L.: "Space Propulsion Systems Utilizing Ignition of Microexplosion by Distant Microexplosion and Some Problems Related to Ignition of Microexplosions by Microexplosions," *Journal of the British Interplanetary Society*, Vol. 53, pp. 62–72, 2000.

15. Lindl, J.D.: *Inertial Confinement Fusion*, Springer-Verlag, New York, 1998.

16. Shmatov, M.L.: "Ignition of Microexplosion by the Laser Pumped by Another Microexplosion," *Journal of the British Interplanetary Society*, Vol. 49, pp. 475–476, 1996.

17. Shmatov, M.L.: "Cyclic Self-Sustaining Process of Thermonuclear Fusion," *Plasma Physics Reports*, Vol. 23, pp. 440–441, 1997.

18. Lindermuth, I.R.; and Kirkpatrick, R.C.: "The Promise of Magnetized Fuel: High Gain in Inertia Confinement Fusion," *Fusion Technology*, Vol. 20, pp. 829–833, 1991.

19. Thio, Y.C.F.; Freeze, B.; Kirkpatrick, R.C.; Landrum, B.; Gerrish, H.; and Schmidt, G.R.: "High-Energy Space Propulsion Based on Magnetized Target Fusion," *AIAA Paper 99–2703*, 1999.

20. Gsponer, A.; and Hurni, J.P.: "Antimatter Induced Fusion and Thermonuclear Explosions," *Atomkernenergie Kerntechnik*, Vol. 49, pp. 198–203, 1987.

21. Lewis, R.A.; Newton, R.; Smith, G.A.; Toothacker, W.S.; and Kanzleiter, R.J.: "An Anitiproton Catalyst for Inertial Confinement Fusion Propulsion," *AIAA Paper 90–2760*, 1990.

22. Lewis, R.A.; Smith, G.A.; Dundore, B.; Fulmer, J.; and Chakrabarti, S.: "Anitiproton-Catalyzed Microfission/Fusion Propulsion Systems for Exploration of the Outer Solar System and Beyond," *AIAA Paper 97–3073*, 1997.

23. Wright, T.P.; Baker, L.; Cowan, M.; and Freeman, J.R.: "Magnetic Flux Compression by Expanding Plasma Armatures," Megagauss Physics and Technology, *Proc. of the Second Int. Conf. on Megagauss Magnetic Field Generation*, P.J. Turchi (ed.), Plenum Press, pp. 241–247, 1979.

24. Cowan, M.; Tucker, W.K.; Wesenberg, D.L.; and Cnare, E.C.: "PULSAR—A Field Compression Generator for Pulsed Power," *Proc. Sixth Symp. on Engineering Problems of Fusion Research, IEEE Pub. No. 75CH1097–5–NPS*, pp. 308–311, 1975.

25. Cnare, E.C.; Wesenberg, D.L.; Cowan, M.; and Tucker, W.K.: "PULSAR—The Experimental Program," *Proc. Sixth Symp. on Engineering Problems of Fusion Research, IEEE Pub. No. 75CH1097–5–NPS*, pp. 312–315, 1975.

26. Cowan, M.; Cnare, E.C.; Leisher, W.B.; Tucker, W.K.; and Wesenberg, D.L.: "Pulsed Energy Conversion with a DC Superconducting Magnet," *Cryogenics*, Vol. 16, No. 12, pp. 699–704, 1976.

27. Cnare, E.C.; Cowan, M.; Wright, T.P.; and Tucker, W.K.: "Pulsed Power Conversion With Inductive Storage," *Proc. Seventh Symp. on Engineering Problems of Fusion Research, IEEE Pub. No. 77CH1267–4–NPS*, pp. 312–315, 1977.

28. Zakharov, Y.P.; Ponomarenko, A.G.; Nakashima, H.; Nagamino, Y.; Nikitin, S.A.; Wolowski, J.; and Woryna, E.: "Direct Energy Conversion of Inertial Confinement Fusion and Experiments With Laser Produced Plasma in Magnetic Fields," *Proc. of the Ninth Int. Conf. on Emerging Nuclear Energy Systems (ICENES '98; Herzliya, Israel)*, Vol. 1, pp. 384–389, 1998.

29. Cha, Y.S.; and Askew, T.R.: "Transient Response of a High-Temperature Superconductor Tube to Pulsed Magnetic Fields," *Physica C*, Vol. 302, pp. 57–66, 1998.

30. Castro, H.; Rinderer, L.; Holguin, E.; and Loude, J.-F.: "Dynamics of Fast Flux Penetration in High-T_c Superconductors," *Physica C*, Vol. 281, pp. 293–302, 1997.

31. Sakharov, A.D.: "Magnetoimplosive Generators," *Soviet Phys.-Uspekhi* (English Translation), Vol. 9, pp. 294–299, 1966.

32. Burnham, M.W.; and Marshall, S.J.: "Some Experiments Related to Explosive Driven MHD Converters," *First Conference on Megagauss Magnetic Field Generation by Explosives and Related Experiments*, Frascati, Italy, H. Knoepfel and F. Herlach (eds.), Euratom publication *EUR 2750.e*, pp. 367–386, 1966.

33. Jaeger, J.C.: "Magnetic Screening by Hollow Circular Cylinders," *Phil. Mag.*, Vol. 29, pp. 18–31, 1940.

34. Weinstein, M.A.: "Magnetic Decay in a Hollow Circular Cylinder," *J. App. Phys.*, Vol. 33, No. 2, p. 762, 1962.

REPORT DOCUMENTATION PAGE

Form Approved
OMB No. 0704-0188

1. AGENCY USE ONLY *(Leave Blank)*	2. REPORT DATE	3. REPORT TYPE AND DATES COVERED
	January 2001	Technical Publication

4. TITLE AND SUBTITLE
Magnetic Flux Compression Reactor Concepts for Spacecraft Propulsion and Power
(MSFC Center Director's Discretionary Fund Final Report; Part I, Project No. 99–24)

5. FUNDING NUMBERS

6. AUTHORS
R.J. Litchford, G.A. Robertson, C.W. Hawk,*
M.W. Turner,* and S. Koelfgen*

7. PERFORMING ORGANIZATION NAMES(S) AND ADDRESS(ES)
George C. Marshall Space Flight Center
Marshall Space Flight Center, AL 35812

8. PERFORMING ORGANIZATION REPORT NUMBER
M–995

9. SPONSORING/MONITORING AGENCY NAME(S) AND ADDRESS(ES)
National Aeronautics and Space Administration
Washington, DC 20546–0001

10. SPONSORING/MONITORING AGENCY REPORT NUMBER
NASA/TP—2001–210793

11. SUPPLEMENTARY NOTES
Prepared for Advanced Space Transportation Program, Space Transportation Directorate
*University of Alabama in Huntsville, Huntsville, AL

12a. DISTRIBUTION/AVAILABILITY STATEMENT
Unclassified-Unlimited
Subject Category 20
Standard Distribution

12b. DISTRIBUTION CODE

13. ABSTRACT *(Maximum 200 words)*

This technical publication (TP) examines performance and design issues associated with magnetic flux compression reactor concepts for nuclear/chemical pulse propulsion and power. Assuming that low-yield microfusion detonations or chemical detonations using high-energy density matter can eventually be realized in practice, various magnetic flux compression concepts are conceivable. In particular, reactors in which a magnetic field would be compressed between an expanding detonation-driven plasma cloud and a stationary structure formed from a high-temperature superconductor are envisioned. Primary interest is accomplishing two important functions: (1) Collimation and reflection of a hot diamagnetic plasma for direct thrust production, and (2) electric power generation for fusion standoff drivers and/or dense plasma formation. In this TP, performance potential is examined, major technical uncertainties related to this concept accessed, and a simple performance model for a radial-mode reactor developed. Flux trapping effectiveness is analyzed using a skin layer methodology, which accounts for magnetic diffusion losses into the plasma armature and the stationary stator. The results of laboratory-scale experiments on magnetic diffusion in bulk-processed type II superconductors are also presented.

14. SUBJECT TERMS
magnetic flux compression, spacecraft, propulsion, power, superconductor, electromagnetics

15. NUMBER OF PAGES
56

16. PRICE CODE
A04

17. SECURITY CLASSIFICATION OF REPORT	18. SECURITY CLASSIFICATION OF THIS PAGE	19. SECURITY CLASSIFICATION OF ABSTRACT	20. LIMITATION OF ABSTRACT
Unclassified	Unclassified	Unclassified	Unlimited